Quaternary Science Reviews 29 (2010) 865–886

Contents lists available at ScienceDirect

Quaternary Science Reviews

journal homepage: www.elsevier.com/locate/quascirev

Controlling factors on a paleo-lake oxygen isotope record (Yammoûneh, Lebanon) since the Last Glacial Maximum

Anne-Lise Develle [a,*], Julien Herreros [b], Laurence Vidal [a], Alexandre Sursock [c], Françoise Gasse [a]

[a] CEREGE, UMR 6635 (Aix-Marseille Université- CNRS-IRD-CdeF), BP 80, 13545 Aix-en-Provence cedex 04, France
[b] Institut de Recherche pour le Développement (IRD), Laboratoire Hydrosciences, UMR 5569, BP 64501 Montpellier cedex 5, France
[c] Centre National de Recherches Géophysiques-CNRS-Liban, Boite postale 165432, Achrafyeh Beyrouth 1100-2040, Lebanon

ARTICLE INFO

Article history:
Received 25 March 2009
Received in revised form
8 December 2009
Accepted 8 December 2009

ABSTRACT

Late Quaternary paleoclimatic changes in the Levant are difficult to extract from carbonate oxygen isotope records partly because the factors controlling the terrestrial $\delta^{18}O$ signals are not fully understood in this region characterized by sharp climatic gradients. Here, we address this purpose by presenting the first ^{14}C-dated isotope record from the northern Levant. The record is based on oxygen isotopes from ostracod shells from lacustrine-palustrine deposits accumulated in a small karstic, hydrologically open basin (Yammoûneh), located on the eastern flank of Mount Lebanon. We have first constructed a composite isotopic record obtained from three different ostracod taxa. This yields an oxygen isotope record of ostracods (δ_{ost}) related to the most widespread species (*Ilyocypris inermis*), and converted to $\delta^{18}O$ values coeval with calcite precipitated in equilibrium (δ_C) with the lake water (δ_L). As with other records from the Mediterranean region, the Yammoûneh profile shows maximum and minimum δ_C values during the LGM and the early Holocene, respectively, and a slight late Holocene increase. In order to discuss the potential causes of the observed $\delta^{18}O$ values fluctuations (e.g., changes in the isotopic composition of the moisture source, temperature, precipitation minus evaporation (P-E) balance, or atmospheric circulation), we tentatively reconstruct the lake water isotope composition by correcting the δ_C values for lake water temperature using regional paleotemperature estimates. Inferred δ_L values were then corrected for the isotopic composition of the Eastern Mediterranean sea surface water (the moisture source) derived from planktonic foraminifera $\delta^{18}O$ values corrected for alkenone-based sea surface temperature. Our study suggests that Holocene δ_L fluctuations are primarily linked to changes in the sea surface water composition (source effect) amplified by enhanced inland rainfall during the early Holocene. During the LGM, low δ_L values at Yammoûneh are likely due to the ground-temperature effect on the rainfall isotope composition, possibly associated with a steeper altitudinal thermal gradient inland, and with changes in air mass trajectories over the Mediterranean Sea.

1. Introduction

The Levant region is located at the transition between the Mediterranean domain and sub-tropical deserts (Fig. 1). The region exhibits steep NS and EW precipitation gradients with high inter-annual to decadal rainfall variability. It is highly sensitive to climatic fluctuations that seriously impact the vulnerable water resources. The moisture source is the Mediterranean Sea. While the coastal zones receive winter rains brought by the mid-latitude westerlies, the marine influence diminishes sharply eastward due to the orographic effect of mountain ranges running parallel to the Eastern Mediterranean Sea coast. There is much interest to reconstruct late Quaternary climatic fluctuations for understanding the mechanisms controlling changes in the regional rainfall pattern which may help validate the hypotheses of causal links between the climate variability and the long history of the Levantine human civilizations (e.g., Bar-Yosef, 1998; Cappers et al., 2002; Issar and Zohar, 2004; Migowski et al., 2006).

The Late Pleistocene–Holocene climate in the Levant has been the focus of a number of studies based on marine and continental records recently synthesized by Robinson et al. (2006) and Enzel et al. (2008). The regional hydrologic picture that is known for this period is largely based on lake level and oxygen isotope records provided from lakes and speleothems. However some caveats remain: (1) there is a marked disparity in spatial coverage between the southern Levant (where well-dated, long-term records provide

* Corresponding author. Tel.: +33 04 42 97 15 81; fax: +33 04 42 97 15 95.
E-mail address: develle@cerege.fr (A.-L. Develle).

0277-3791/$ – see front matter © 2009 Elsevier Ltd. All rights reserved.
doi:10.1016/j.quascirev.2009.12.005

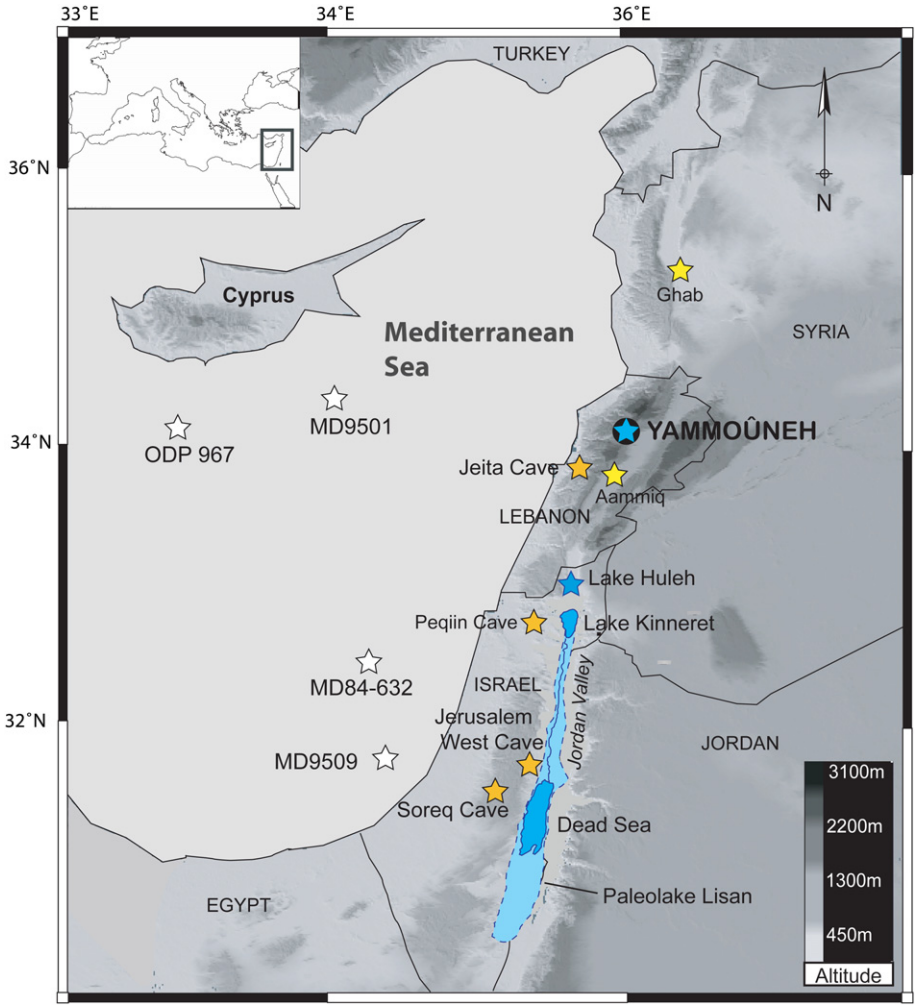

Fig. 1. Map of the Levant region showing the location of Yammoûneh and of sites of Late Pleistocene–Holocene paleoclimatic records cited in the text. Records derived from lake level reconstructions (in blue), speleothems (orange stars), pollen (yellow stars) and marine cores (white stars). Note that the area of paleo-Lake Lisan shown here (from Kolodny et al., 2005) is that of its maximum extent (26–24 ka; Bartov et al., 2003).

detailed information on the glacial–interglacial cycles, and the northern Levant where only one Holocene $\delta^{18}O$ record exists, and (2) the factors controlling the $\delta^{18}O$ of lakes and cave waters are still intensively debated in the region.

In the southern Levant (see Fig. 1 for site locations), reconstructions of lake-level fluctuations over the past 70 ka in the Jordan Valley–Dead Sea basin demonstrate much wetter conditions during the last glacial period (until 26 or 17 ka) than during the Holocene, i.e., the paleo-Lake Lisan (Bartov et al., 2002, 2003; Haase-Schramm et al., 2004; Bookman et al., 2006; Lisker et al., 2009), Lake Kinneret (Hazan et al. (2005) and the Dead Sea (Enzel et al., 2003; Migowski et al., 2006; Torfstein et al., 2009a) (Fig. 2a). Average $\delta^{18}O$ values of aragonite laminae in Lake Lisan–Dead Sea sediments are 2–3‰ heavier during the last glacial period compared to the Holocene period (Fig. 2b; Kolodny et al., 2005). Continuous speleothem $\delta^{18}O$ records from central Israel, e.g., the West Jerusalem Cave (Frumkin et al., 1999, 2000) and Soreq Cave records (Fig. 2c), also show high/low $\delta^{18}O$ values during the last glacial/interglacial periods, respectively, and mimic $\delta^{18}O$ fluctuations of planktonic foraminifera in marine cores from the eastern Mediterranean Sea (Fig. 2d). Interpretations of terrestrial $\delta^{18}O$ records put forward different controlling factors of the $\delta^{18}O$ signal, sometimes leading to conflicting paleoclimatic conclusions. According to Frumkin et al. (1999, 2000), Kolodny et al. (2005), Enzel et al. (2008), and Torfstein et al. (2009b), long-term changes in $\delta^{18}O$ carbonate records primarily reflect the changes of isotopic composition of the water vapor source (the so-called "source effect"). During the last glacial period, which was wet (as indicated by Lake Lisan highstands), high $\delta^{18}O$ values were attributed to the isotopic enrichment of the Eastern Mediterranean (EM) sea waters due to the global ice volume effect. On another hand, long-term fluctuations in speleothem $\delta^{18}O$ records from Soreq and Peqiin Caves have been initially interpreted as primarily reflecting the "amount effect" and "temperature effect" (Dansgaard, 1964; Rozanski et al., 1992, 1993), i.e., high/low $\delta^{18}O$ values indicate dry-cold glacial/wet-warm interglacial periods, respectively (Bar-Matthews et al., 1997, 1999, 2003). This view suggests dry/wet Last Glacial/Holocene conditions, in contradiction with lake-level records.

In the northern Levant, the unique $\delta^{18}O$ record comes from a well-dated Holocene speleothem from the Jeita Cave in Lebanon, which shows obvious similarities with the Soreq Cave record (Nader et al., 2007; Verheyden et al., 2008; Fig. 2c). Following Bar-Matthews et al. (2003), high/low $\delta^{18}O$ values were attributed to high/low rainfall amount.

Recently, Almogi-Labin et al. (in press) compare new marine $\delta^{18}O$ records from the northern (MD9501) and southern (MD9509) Levantine basin, respectively, to Soreq Cave data over the past 90 ka. These authors conclude that, superimposed on the source

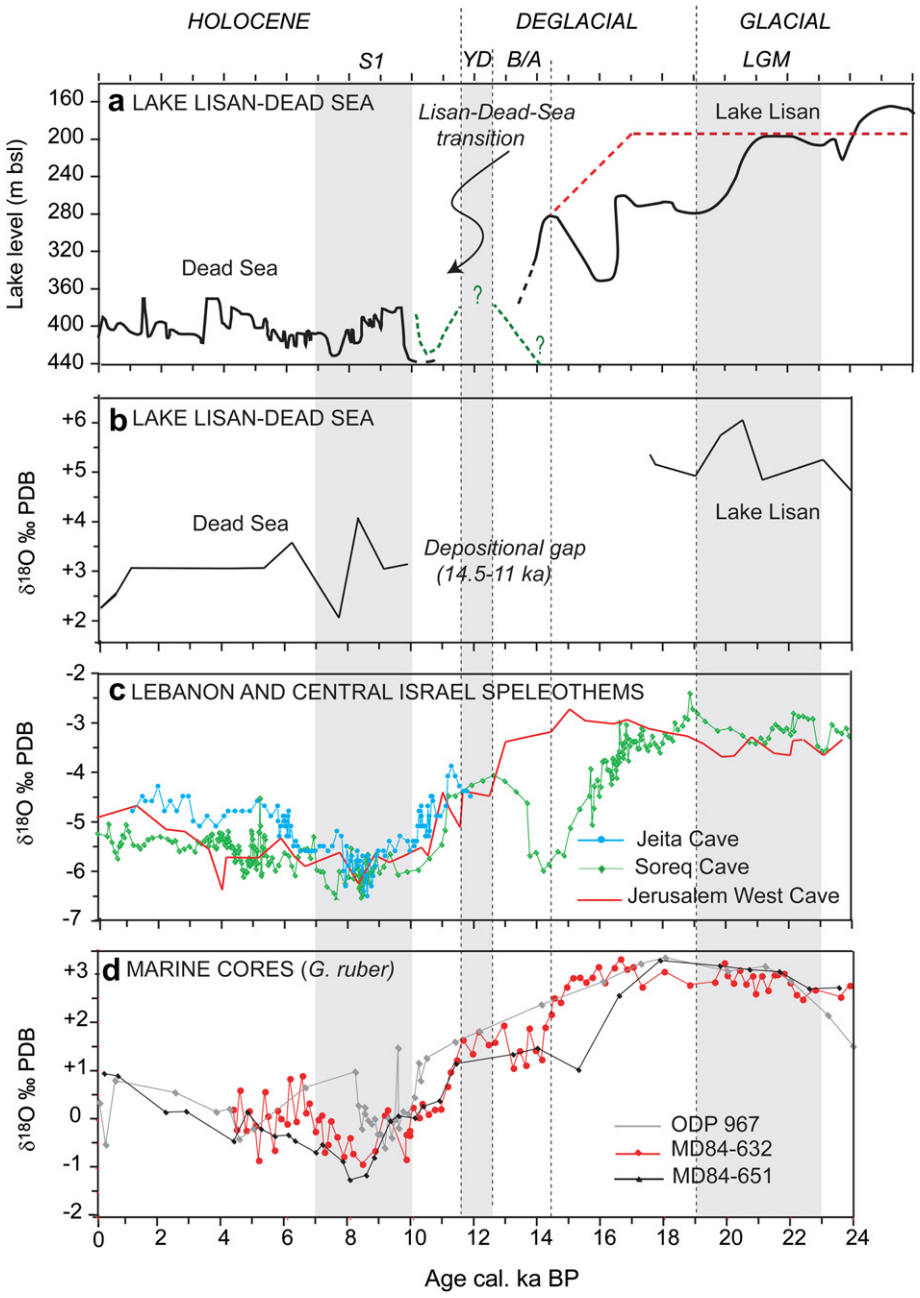

Fig. 2. Records from the Levantine region illustrating climatic changes since the last glacial period. (a) Lake Lisan–Dead Sea level fluctuations. Black curves after Bartov et al. (2003), Migowski et al. (2006), Bookman et al. (2006); dashed red line after Lisker et al. (2009); dashed green line after Torfstein et al., 2009a. (b) $\delta^{18}O$ data of aragonite laminae from Lake Lisan–Dead Sea (after Kolodny et al., 2005). (c) $\delta^{18}O$ records of speleothem carbonates from Jerusalem West Cave (red, after Frumkin et al. 1999) and Soreq Cave (black, Bar-Matthews et al., 2003) in central Israel, and from Jeita Cave in Lebanon (green, Verheyden et al., 2008). (d) $\delta^{18}O$ records of planktonic foraminifera *Globigerinoides ruber* in marine cores: MD84-651 (green, Fontugne and Calvert, 1992); ODP 967 (gray, Emeis et al, 2003); MD84-632 (red, Essallami et al., 2007). Vertical gray bands: specific time intervals. LGM, Last Glacial Maximum (Mix et al., 2001). B/A, Bölling-Alleröd; YD, Younger Dryas, as defined from polar ice cores (e.g., Blunier and Brook, 2001). S1, Sapropel 1 deposition in the Mediterranean Sea (e.g., Röhling, 1994).

effect, rainfall amount has an important impact on rainfall $\delta^{18}O$ values during interglacial periods, while increased continentality and altitude effects may have acted to decrease the rainfall $\delta^{18}O$ during glacial periods. These authors also point out the important contribution of the Nile River discharge on the values of $\delta^{18}O$ EM water during periods of high monsoonal activity, and time intervals with N–S $\delta^{18}O$ and temperature gradients significantly different from today in the Levantine basin.

In order to depict possible spatial paleohydrologic heterogeneity in the Levantine region since the Last Glacial Maximum (LGM; 21 ± 2 ka; Mix et al., 2001) and to disentangle the interlinked processes acting on inland rainfall and carbonate $\delta^{18}O$ values, we provide the first ^{14}C-dated $\delta^{18}O$ record covering the LGM in the northern Levant. The present study focuses on $\delta^{18}O$ values of ostracod valves used as an indicator of paleohydrologic regime in a small karstic, hydrologically open freshwater lake basin from Lebanon (Yammoûneh basin) and addresses the following questions:

(1) What are the dominant factors controlling the $\delta^{18}O$ composition of lake water and carbonates in this open lake during the LGM and the Holocene, respectively?

(2) How does the Yammoûneh record compare with other carbonate $\delta^{18}O$ records from the region?

The Yammoûneh ostracod $\delta^{18}O$ record was first corrected for the species-dependent fractionation factor (the "vital effect") to obtain values coeval with theoretical $\delta^{18}O$ of inorganic calcite precipitated in isotopic equilibrium with ambient lake water. Then, taking advantage of working on a lake system with rapid through flow where evaporative isotopic concentration is small or negligible, we tentatively correct our carbonate $\delta^{18}O$ values for the effect of water temperature, using paleotemperatures inferred from different proxies in the region. The resulting profile, theoretically representing changes in the paleo-lake water isotopic composition, is compared to temperature-corrected $\delta^{18}O$ values of cave water time series from the northern and southern Levant, and to $\delta^{18}O$ fluctuations of eastern Mediterranean sea surface water. Although based on several assumptions, our approach allows us to discuss the relative role of the "source effect" versus changes in temperature, rainfall amount, and possibly in storm-track trajectories linked to global glacial/interglacial reorganization in atmospheric circulation.

2. Environmental setting

The 6 km long, 2 km wide Yammoûneh basin (34.06°N–34.09°N, 36.01°E–36.03°E, 1360 meters above sea level (m a.s.l)) is located on the eastern flank of Mount Lebanon, about 37 km from the Mediterranean Sea shore (Fig. 3a). Since at least Roman times (Besançon, 1968), a shallow seasonal lake occupied the southern part of the basin (Yammoûneh means little sea in classical Arabic). However, this lake was drained in the early 1930s following the construction of an underground duct designed to transport water for irrigation of the Beqaa plain located eastward. Before this man-made drainage, a seasonal lake developed in March–April for a mean duration of 5 months and might have reached a depth of 2 m (dry years) to 10 m (wettest years) (Abd-el-Ab, 1967; Besançon, 1968). The basin floor is today entirely cultivated.

2.1. Geological setting

The Yammoûneh depression is a tectonic (pull-apart) basin along the Yammoûneh Fault, which is a major branch of the active Levant Fault System (Daëron et al., 2004, 2007; Daëron, 2005). The basin's long axis strikes NNE–SSW, roughly parallel to the Mediterranean coastline and to the major Lebanon geographical structures (Fig. 3a): from west to east, a narrow coastal plain, the Mount Lebanon chain culminating at 3083 m a.s.l., the Beqaa Valley at ~900 m a.s.l., and the Anti-Lebanon Mountains chain at 2000 m a.s.l. The Yammoûneh basin (Fig. 3b) is inset between thick sub-tabular sequences of intensively karstified Cenomanian limestones (Dubertret, 1975; Hakim, 1985). West of Yammoûneh, the karstic Mnaïtra plateau rises abruptly to 2100 m a.s.l. To the East, the basin is separated from the Beqaa Valley by gently sloping hills (Jabal el-Qalaa, ~1500 m a.s.l.). Patches of whitish lacustrine deposits apparent in the southern part of the basin indicate the ancient lake area, while coarse clastic deposits mostly brought by the Aïnata River (a small tributary flowing from the eastern flank of Mt Lebanon) overlie the Cenomanian limestone bedrock in the northern part (Besançon, 1968).

2.2. Climatic setting

The Lebanese climate is Mediterranean with cool, wet winters and hot, dry summers. The influence of the mid-latitude westerlies dominates during winter while high pressure systems centered over Iraq and Iran produce the summer weather. The Mount Lebanon ridge plays a major role on climate. Precipitation and temperature vary considerably in relation with the topography and distance from the sea (Service Météorologique du Liban, 1977; Abi-Saleh and Safi, 1988; Karam, 2002) (Fig. 4a). The transition from a humid coastal zone to the desert occurs in less than 200 km from west to east. Mean annual precipitation (MAP) ranges between 700 and 1000 mm along the coast to >1400 mm in Mount Lebanon; it decreases to 400 mm in the Beqaa plain and less than 200 mm in the north-east. Above 2000 m a.s.l., precipitation is essentially niveous. The Mnaïtra plateau remains completely snow-covered

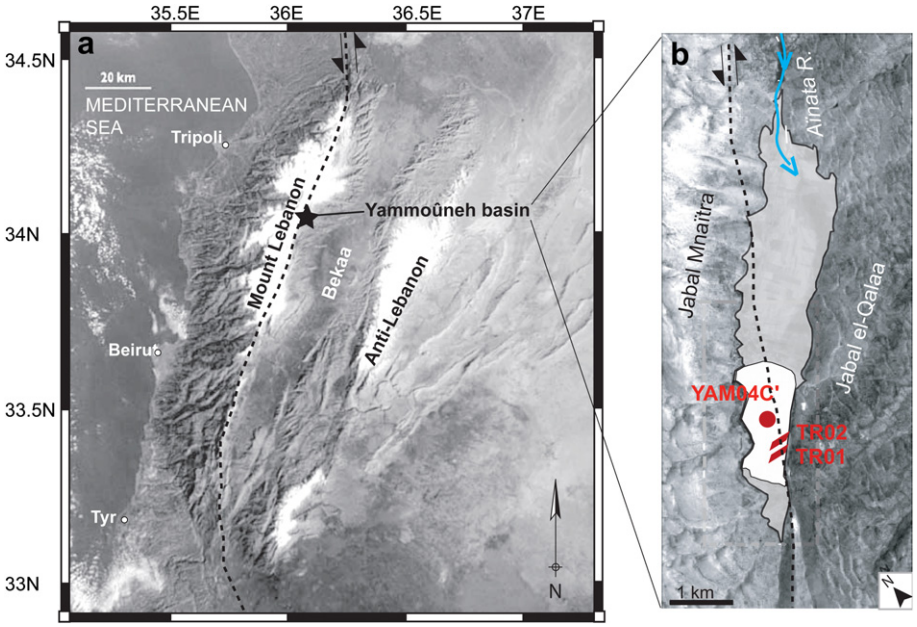

Fig. 3. The Yammoûneh basin in Lebanon observed from satellite (SPOT images). (a) Main morphological structures of the country. (b) The Yammoûneh depression and approximate paleolake area (in white) with location of the sedimentary profiles TR01 and TR02 (trenches) and YAM04C′ (piston core). The black dashed line is the surface trace of the Yammoûneh Fault; black arrows show the direction of lateral movement along the fault (modified from Daëron, 2005).

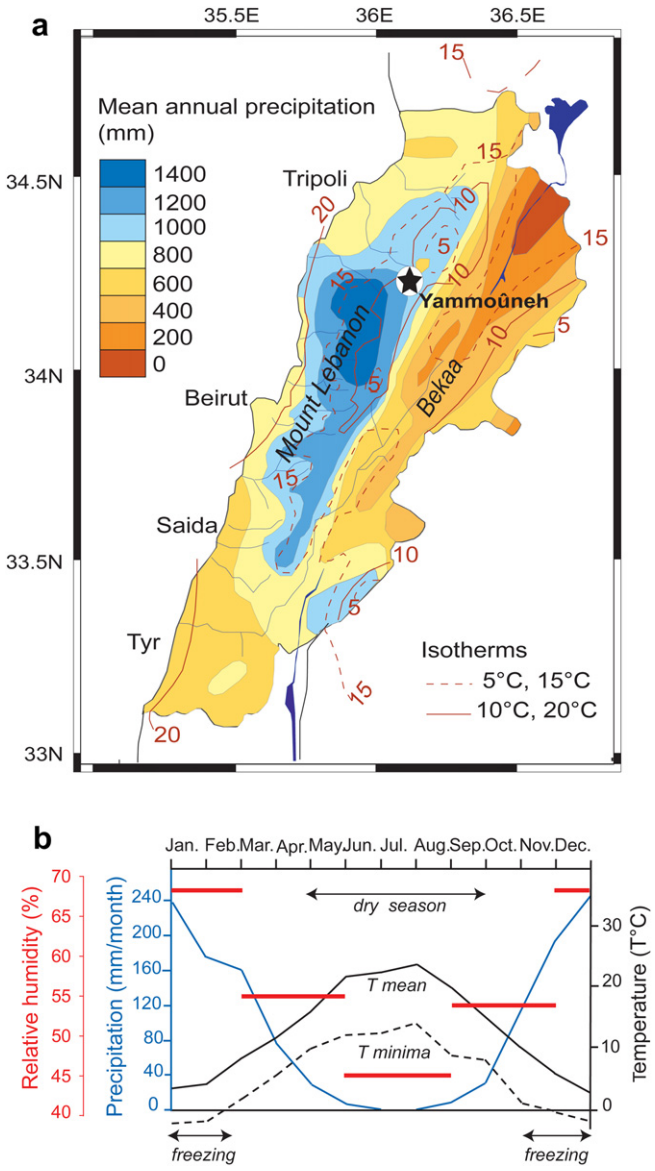

Fig. 4. Climate setting. (a) Mean annual precipitation and temperature over Lebanon (after Abi-Saleh and Safi, 1988). (b) Monthly mean precipitation and temperature, and seasonal change in relative air humidity at Yammoûneh (Service Météorologique du Liban, 1977).

almost 4 months a year. The seasonal thermal contrast is high and increases with continentality.

At Yammoûneh (Besançon, 1968; Service Météorologique du Liban, 1977; Safi and Abi-Saleh, 1999), the rainfall regime resembles that of the western flank of Mount Lebanon, but continentality is marked by huge diurnal and seasonal variations in temperature and relative air humidity (Fig. 4b). MAP reaches 900–1000 mm/year, as snow falls over about 30 days/year. The dry season lasts 5 months. Mean annual temperature (MAT) is about 15 °C. Mean of temperature minima of the coldest month is −4.2 °C and mean of temperature maxima during the warmest month reaches 34.6 °C. Freezing occurs over 3 months/year. Relative humidity varies between about 70% in winter and 45% in summer.

2.3. Hydrology

In order to interpret the isotopic composition of lacustrine ostracod shells, one must first consider the major components of the paleolake water balance. Besides direct precipitation (<1.2 10^6 m^3/year), the Yammoûneh basin largely depends on precipitation over the western highlands. The basin receives runoff water from the surrounding mountain slopes and from the Aïnata River, but the most important inflow comes from permanent karstic springs (35–70 × 10^6 m^3/year; Besançon, 1968; Hakim, 1985). Beneath the Mnaïtra plateau, subterranean karstic networks collect snow melt-water feeding a dozen springs along the western edge of the basin. The spring discharge reaches its maximum in late spring–early summer but delivers relatively cold freshwater all year round. Following the smooth slope of the basin, sinuous channels drain spring and runoff water into karstic sinkholes along the opposite eastern border. The karstified, intensively fissured and faulted Yammoûneh depression is highly permeable. The basin is thus hydrologically open despite the absence of surface outlet. Leakage through the basin floor has always reduced the lake water residence time and its enrichment in salt and heavy isotopes.

The Mnaïtra-Yammoûneh karstic system is poorly known, but data from nearby underground systems lying in the same Cenomanian limestone formation and with similar high hydraulic gradients suggest that the Yammoûneh spring water comes from recent winter precipitation in the Mnaïtra highlands. An isotope study of the snow cover and karstic spring water from the western flank of Mount Lebanon has shown that snow melt-water rapidly recharges the karstic aquifers in spring and early summer without significant distortion by evaporation or sublimation processes (Aouad et al., 2004). In the Jabal el-Qalaa karstic system (Fig. 3b), the average water residence time was estimated at 1.5–3 years and the karstic spring water along the western margin of the Beqaa plain (Fig. 3a) exhibits oxygen isotope values very similar to those of the highest winter rainfalls in the mountain without significant seasonal variations (el Hakim, 2005). In such systems, the response time of the spring discharge to precipitation variability is negligible on the geological time scale.

2.4. Origin and isotopic composition of regional precipitation

Spatial and seasonal distributions of modern rainfall in the Levant are controlled by the Mediterranean Sea (Sharon and Kutiel, 1986; Gat et al., 2003). The winter rain is formed within cold air masses of European or Atlantic origin which sweep across the Mediterranean and gain moisture while moving over the warmer sea waters. Most of the annual rainfall comes from an extratropical cyclone, the Cyprus Low, formed in the eastern Mediterranean (EM), or a rejuvenation of a depression formed previously in the central Mediterranean in its eastward movement, although westerly flow may also contribute (Fig. 5a). The intersection of the northwesterly–westerly flow with the shoreline and, later on, with the mountain ridges, results in intensive rainfall over the region. Interannual to decadal variations are superimposed on the seasonal scale. Changes in the NS precipitation gradient are linked to changes in air mass trajectories associated with sea-level pressure and sea surface temperature (SST) anomalies, which are in turn related to the upper-level (500 mbar) pressure pattern over the Mediterranean Sea (Enzel et al., 2003; Zangvil et al., 2003; Ziv et al., 2006).

The oxygen and deuterium isotope compositions of precipitation ($\delta^{18}O$ and δD) in the Levant are primarily determined by the intensity of the sea–atmosphere interaction occurring over the Mediterranean Sea, which depends on, among others, the air–sea temperature differences and the duration of interaction (Gat and Carmi, 1970; Gat, 1996; Gat et al., 2003). In the EM region, the relatively strong interaction results in a high deuterium excess ($d = \delta D - 8 \times \delta^{18}O = 22‰$) and a EM meteoric water line (MMWL; Gat and Carmi, 1970, 1987) slightly above the global meteoric water line (GMWL; Craig, 1961), as seen for some stations of Lebanon

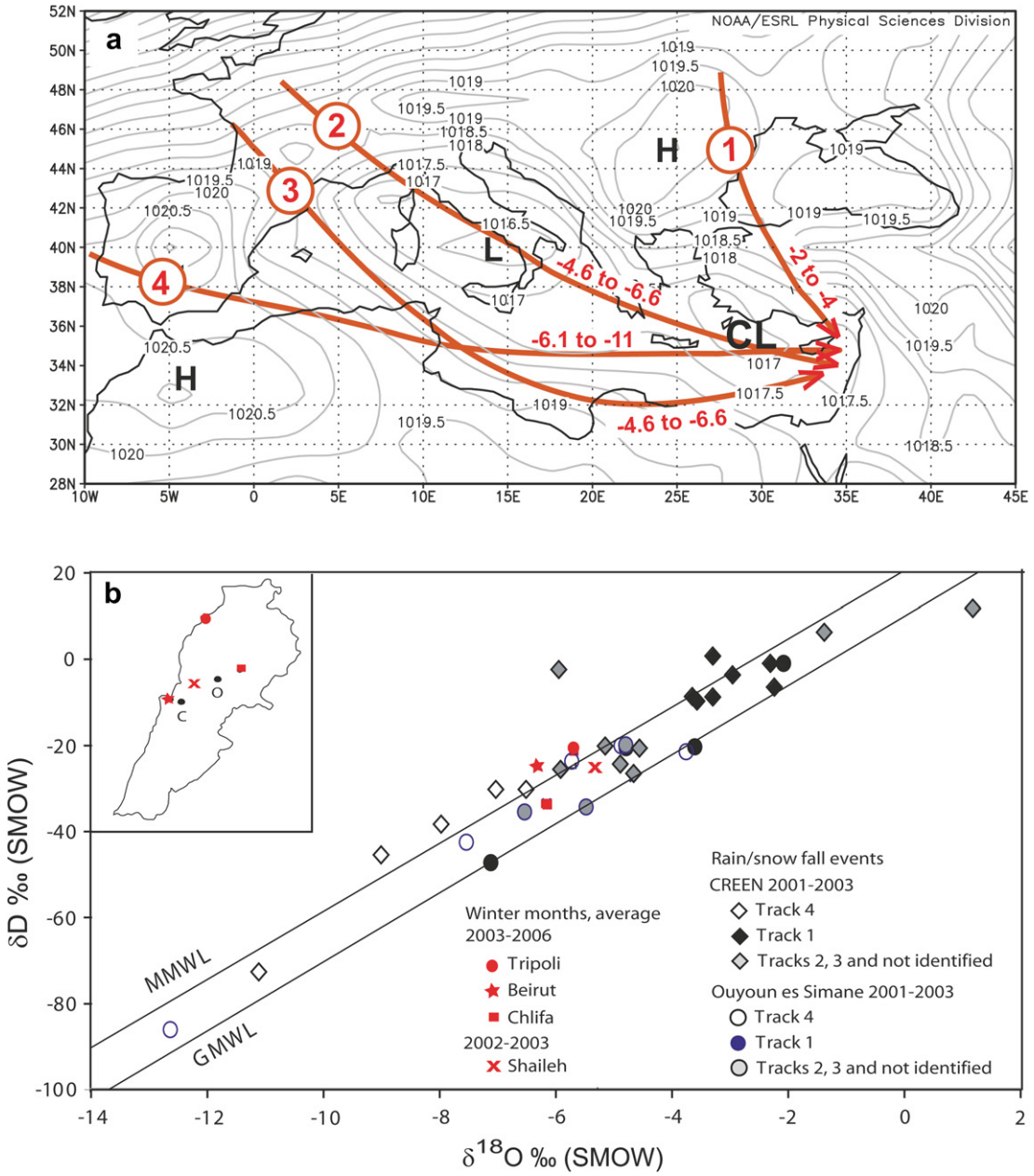

Fig. 5. Origin and isotopic composition of precipitation. (a) Long-term mean (1968–1998) of December–January–February sea-level pressure in the Mediterranean region, in millibars (extracted from the NOAA climate diagnostic center, Boulder, Colorado, http://www.cdc.noaa.gov/). Note the low pressure cells south of Turkey (the Cyprus Low, CL) and in central Mediterranean south of Italy (L). In red: trajectories of air masses which have produced rains over the western flank of Mount Lebanon during the winters 2001–2003, and corresponding $\delta^{18}O$ isotopic composition of precipitation close to Beirut (CREEN station; after Aouad et al., 2005). (b) Average isotope values for winter months (in red) at four Lebanese stations close to Yammoûneh (GNIP data, IAEA-WMO, http://nds121.iaea.org/wiser/); isotopic signal of individual rainfall events at the CREEN station, 249 m a.s.l., and snow events at Ouyoun es Simane, 1860 m a.s.l. (Aouad et al., 2004, 2005). The inset in (b) shows the station location (C: CREEN, O: Ouyoun es Simane,). GMWL, global meteoric water line; MMWL, Mediterranean meteoric water line.

(data from the Global Network of Isotopes in Precipitation, GNIP; http://isohis.iaea.org; Fig. 5b).

The $\delta^{18}O$ and δD values of individual rainfall events have been related to the origin and flow direction of air masses on the basis of stable isotope measurements coupled with air mass trajectory synoptic back-tracking from meteorological and satellite data. Observations were conducted during one rainfall season (1980–1981) at one station from southern Israel (Rindsberger et al., 1983, 1990) and two rainfall seasons (2001–2003) at four stations of different altitudes (28–1860 m a.s.l.) along the western flank of Mount Lebanon (Aouad et al., 2004, 2005). Results are not fully consistent, possibly due to the short time period investigated or to regional and interannual differences. In Lebanon, four groups of trajectories have been identified (Figs. 5a,b). Close to Beirut (CREEN station, 249 m a.s.l.), the most ^{18}O-depleted rain (-6.1 to $-11‰$) was associated with air masses from the west having a long path over the sea (track 4 in Fig. 5a). The most enriched rains ($\delta^{18}O = -2$ to $-4‰$) originated from continental arctic air, which flows over a very short distance over the warm EM (track 1 in Fig. 5a). The same trend was observed for snow events at Ouyoun es Simane (1860 m a.s.l., Fig. 5b). Local climatic factors induce, however, high temporal and spatial variability. Low intensity rains are often

affected by evaporation processes in the air column especially at the beginning and end of the rainy season.

On the annual time scale, the "rainfall amount, ground temperature, altitude and continentality effects" (Dansgaard, 1964; Rozanski et al., 1992, 1993) exert important controls on mean rainfall isotopic composition. Isotopic values extracted from the interpolation model based on GNIP data (Bowen and Wilkinson, 2002; Bowen and Revenaugh, 2003; http://www.waterisotopes.org/) along a WE transect crossing the Yammoûneh basin (Fig. 6a) show that the isotopic composition of precipitation fingerprints the climate gradients with increasing depletion from the EM coast toward the interior and as elevation increases (Fig. 6b). According to this model, the weighted mean annual precipitation $\delta^{18}O$ values is close to -8‰ at Yammoûneh, -5.5 ‰ at the coastal site (Jubayl) and -9.5‰ at the highest, coldest and wettest site (El Aarîch). As more than 90% of the precipitation falls in winter, the mean of the December-March values (Fig. 6c) is very close to the weighted annual mean. Monthly $\delta^{18}O$ values estimated at Yammoûneh (Fig. 6d) follow the seasonal cycle of rainout and temperature (Fig. 3b), with increasing depletion from November to January (the wettest month). Small rains of the warmer seasons are shifted toward the GMWL suggesting evaporation in a dry atmosphere. Summer data extracted from the model are poorly reliable due to the unevenness of data and the extreme scarcity of summer rainfall events in the region (Fig. 4b).

3. Materials and methods

3.1. Trench and core material

Two trenches (Fig. 3) were dug: one in 2001 (TR01; 5-m deep, 75-m long) and one in 2002 (TR02; 9-m deep, 50-m long) for neotectonic investigation in the framework of French–Lebanese collaborative programs (CEDRE, French Embassy in Beirut and CNRS-L). TR01 has been already described and dated by Daëron et al. (2007). For paleoclimatic reconstruction, the TR02 section was sampled at 1–5 cm intervals along vertical profiles undisturbed by the Yammoûneh fault activity. In 2004, coring was performed (SEDIDRILL Mazier and cable corers) to collect longer sedimentary sequences. The longest core (YAM04C′, 73 m; Fig. 3) likely covers the complete basin infilling.

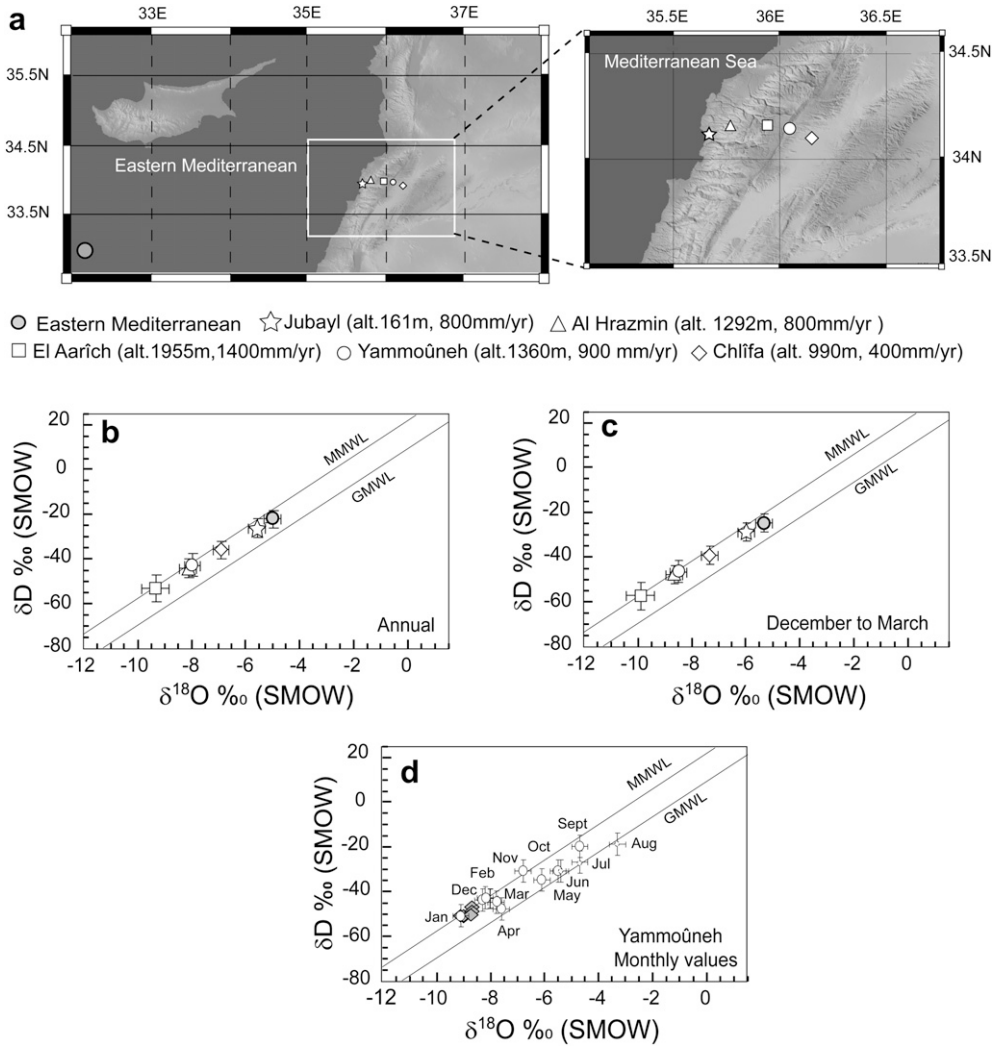

Fig. 6. $\delta^{18}O$ and δD composition of precipitation along a W–E transect from the Mediterranean Sea to the Beqaa plain, extracted from the interpolation model of Bowen and Wilkinson (2002) and Bowen and Revenaugh (2003); http://www.waterisotopes.org/. (a) Location of selected sites. (b) Weighted mean annual values. (c) Average values for the wet season. (d) Monthly values at Yammoûneh compared to the isotopic composition of Yammoûneh karstic spring and aquifer water (gray diamonds) collected in September 2004 (see Table 2). Error bars: confidence intervals calculated from the Bowen et al. (2005) program.

This paper concerns the upper part of TR02 and YAM04C′. The TR01 profile is mainly used to support the chronology of remarkable stratigraphic layers observed in the three sedimentary sections.

Measurements of the total magnetic susceptibility (K) in TR02 and of YAM04C′ were performed using a Bartington MS2 susceptibility meter at CEREGE on cubic 8 cm^3 discrete samples at intervals of 1–10 cm in TR02 and 5 cm in the upper 150 cm of core YAM04C′, and every 1 cm below 150 cm in the core.

3.2. Radiocarbon dating

AMS-^{14}C dating was performed on water and wood samples. The ^{14}C activity of total dissolved inorganic carbon (TDIC) in four spring water samples was measured at LMC14, CEN Saclay, Gif-sur-Yvette. In the sediments, where no leaf or seed of terrestrial plants was found, radiocarbon dating was performed on partly carbonized macroscopic wood fragments from samples undisturbed by bioturbation or fault activity. Wood fragments were relatively abundant in the SI series of the trench walls close to the eastern shore, but extremely rare in SII. In the core, located in the central part of the depression and of small diameter (10 or 6 cm), sediments are almost devoid of datable material. For the upper 5 m of the sections, 19 wood samples were found in TR01 (Daëron et al., 2007), 6 in TR02 and 1 in YAM04C′. Wood fragments were cleaned of the surficial millimeters and subjected to acid/base pretreatment to remove carbonate and percolated organic acids and to minimize potential biases by diagenesis. Reworking of wood fragments by stripping of the soil cover caused by massive rainstorms cannot, however, be excluded.

The ^{14}C ages were converted into calendar years (2σ standard deviation) using the terrestrial calibration curve IntCal04.14 (Reimer et al., 2005). In addition, we used the Bchron model (Haslett and Parnell, 2008), which calculates all possible sedimentation rates to estimate uncertainties between two dated points.

3.3. Isotope analyses

3.3.1. Water samples

Six water samples were collected for $\delta^{18}O$ and δD analyses in autumn 2004 from four karstic springs, a small pool (close to the major eastern sinkhole and to the Aïnata river mouth), and an aquifer reached at 22 m deep during coring. Samples have been equilibrated successively with H_2 and CO_2 gas in an automated Thermo-Finnigan equilibrating unit, and measured on a dual inlet Delta Plus mass spectrometer at CEREGE. Results are reported in delta values, representing deviations in per mil (‰) from V-SMOW. The reproducibility of these measurements is ±0.05‰ and ±1‰ (1σ) for $\delta^{18}O$ and δD respectively.

3.3.2. Ostracods samples

Well-preserved ostracod valves occur throughout the sedimentary profiles except in a few short intervals. Stable isotopic compositions in benthic ostracods were determined in TR02 and YAM04C′ samples. Since no one ostracod taxon occurs in sufficient number along the studied profiles, analyses were performed on the three most abundant taxa: *Ilyocypris inermis* (the most widely distributed which dominates in SI deposits), *I. gibba,* and *Candona neglecta* (only found in the Holocene series where it is mainly represented by juvenile forms). Because the lake is presently dry, neither lake monitoring nor calibration on modern material from Lake Yammoûneh could be performed.

I. inermis is a littoral species most commonly found in springs from mountainous areas and associated ponds, watercourses and small lakes. It survives desiccation and often dominates in ephemeral waterbodies. It has two generations per year (in spring and autumn) and is found all year round (Wolf, 1920; Roca and Baltanàs, 1993; Mezquita et al., 1999; Meisch, 2000; Külköylüolu and Yilmaz, 2006). *I. gibba* is characteristic of small and shallow permanent bodies, although it can occur in temporary pools and tolerate slightly saline water. It produces two annual generations, but individuals are more abundant in late spring and summer than during the winter (Mezquita et al., 1999; Meisch, 2000; Wilkinson et al., 2005). *C. neglecta* is an ubiquitous benthic form generally found in lakes, but also encountered in spring water or temporary waterbodies (Bronshtein, 1947; Filippi et al., 1999; Meisch, 2000; Ricketts et al., 2001; Belis and Ariztegui, 2004; Wilkinson et al,. 2005; Külköylüolu and Yilmaz, 2006; Dügel et al., 2008). *C. neglecta* was found in association with *I. inermis* in Turkish springs (Külköylüolu and Yilmaz, 2006). It prefers cool water but tolerates short periods of temperature increase beyond 20 °C. The species has two annual generations (Wolf, 1920). In the littoral zones of lakes from North Germany, Hiller (1972) showed that adults appear only in autumn and winter whereas juveniles are present all year round.

After wet sieving, the sediment fraction >150 μm was dried at 40 °C, and ostracod valves of these three taxa were hand-picked under a stereo microscope. After a few seconds in an ultra-sonic bath, which help the elimination of detrital particles, valve cleaning was finally controlled under the microscope. The determination of $\delta^{18}O$ and $\delta^{13}C$ values was performed on CO_2 resulting from the reaction of the valve carbonate with H_3PO_4 acid at 70 °C, with a Finnigan Delta Advantage mass spectrometer at CEREGE. This system requires a minimum of 60 μg of $CaCO_3$ (corresponding to eight valves of juvenile *C. neglecta* and five valves of *Ilyocypris* sp.). Stable isotopic ratios are expressed in ‰ relative to the V-PDB standard. A total of 87 levels (54 for TR02 from 10.5 to 455 cm, 33 for YAM04C′ from 63 to 500 cm) have provided sufficient material for analyses.

Analytical precision of $\delta^{18}O_{ost}$ and $\delta^{13}C_{ost}$ is ±0.04‰ and ±0.02‰, respectively, based on repeated analyses of a NBS-19 limestone standard (−2.2‰ and +1.95‰ for $\delta^{18}O$ and $\delta^{13}C$, respectively).

4. Results

4.1. Lithostratigraphy

Simplified stratigraphic logs of TR01 and of the 5 upper meters of TR02 and of YAM04C′ are presented in Fig. 7. A more detailed description of the TR02 and YAM04C′ lithofacies, based on macroscopic and smear-slide observations, is given in Supplementary Appendix A. Magnetic susceptibility (K) records for TR02 and YAM04C′ are shown in Fig. 8.

The most striking sedimentary change observed in the 3 sedimentary profiles is a transition from an upper series, SI, which consists of a pale lacustrine chalk and known to be of Holocene age from ^{14}C dates of TR01 (Daëron et al., 2007), to a relatively uniform series of yellowish-brown to dark brown clayey silt, SII. The SI Holocene chalk is rich in valves of a diversified ostracods fauna associated with abundant shells of gastropods, charophytes, calcified tests of Chlorophyceae algae, fragments of aquatic plants, all reflecting a freshwater, generally shallow lake. The SI series exhibits low and rather stable magnetic susceptibility values ($K < 25 \times 10^{-10}$ m^3). Conversely, in SII, the mineral fraction of detrital origin dominates in material with high and fluctuating susceptibility values ($K > 50 \times 10^{-}5$ m^3). Several indurated, strongly oxidized layers, beds of calcareous concretions likely of pedogenic origin and a paleochannel (in TR02) indicate frequent periods of desiccation or hiatus in sedimentation. Remains of freshwater organisms are rare and poorly diversified. In the trenches, the SI–SII transition is abrupt, at 199–200 cm in TR02

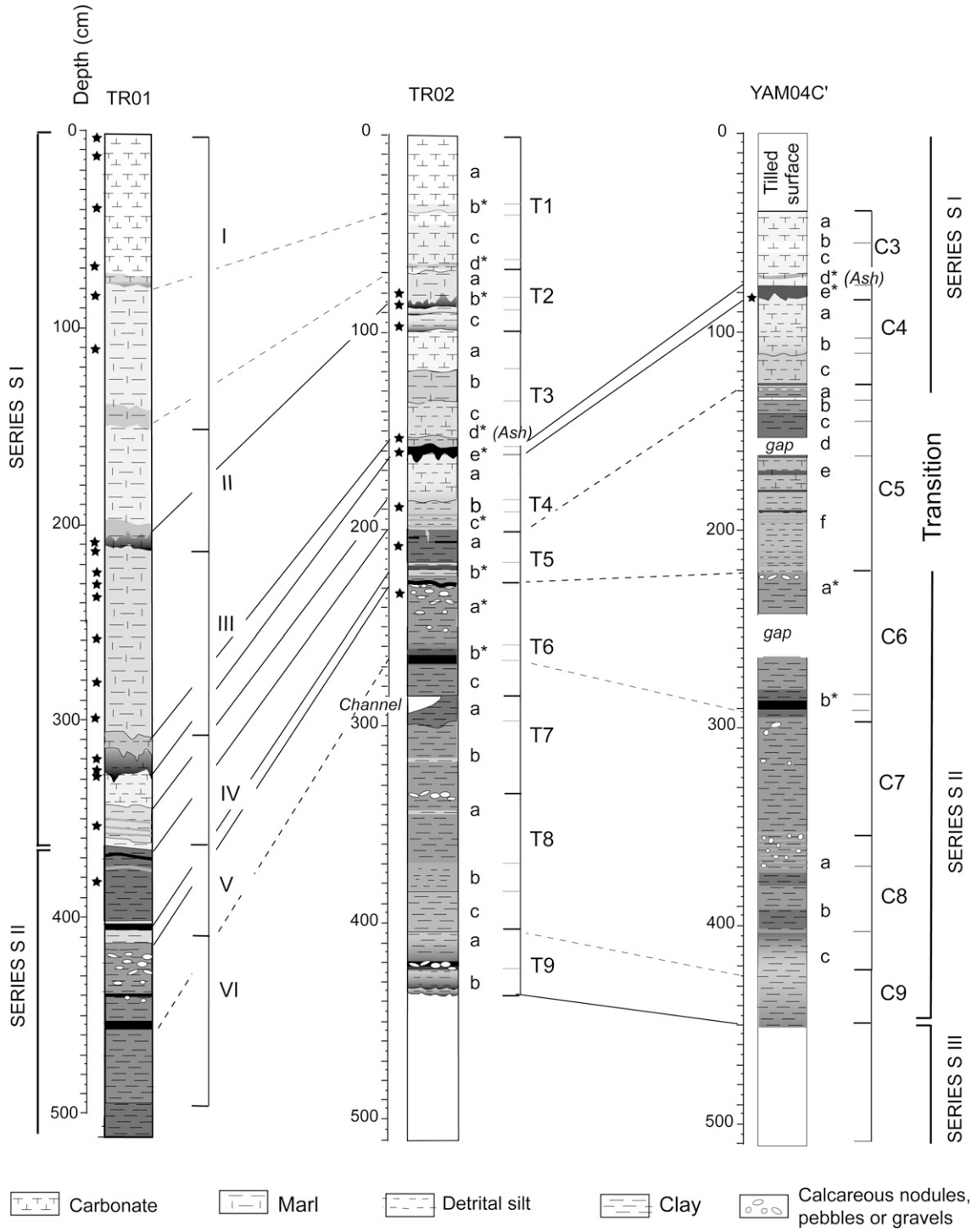

Fig. 7. Simplified stratigraphic logs of TR01 (after Daëron et al., 2007), TR02 and YAM04C′. The gray scale represents color intensity (from white to dark brown and black). The two gaps in YAM04C′ are due to coring problems (loss of sediments at the base of core sections, no sediment recovery). Ash, position of the ash layer observed in TR02 and in the core (see Develle et al., 2009); black stars, levels with radiocarbon dates, oblique lines, evident (full lines) or hypothesized (dashed lines) correlations between stratigraphic columns based on lithofacies. See details in Supplementary Appendix A.

(units T5–T4 boundary) and at 412 cm in TR01 (sequences V–VI boundary). It is more progressive (between 127 and 220 cm) in the core. Differences in the SI thickness between profiles are likely due to the topography of the basin floor, the proximity to eastern shore, and local sedimentation/erosion processes. TR02 and YAM04C′ have revealed that SII overlies a thick sequence of very characteristic olive gray clay (SIII) below ~435–450 cm.

Apart from these first-order variations, subtle changes in color, texture and composition allow units and sub-units to be defined. The most distinctive layers (marked by an asterisk in Fig. 7 and Supplementary Appendix A) were used as marker beds for level-to-level stratigraphic correlations between the sedimentary columns (see details in Supplementary Appendix A). Most of the remarkable layers observed in TR02 were clearly identified in the nearby TR01

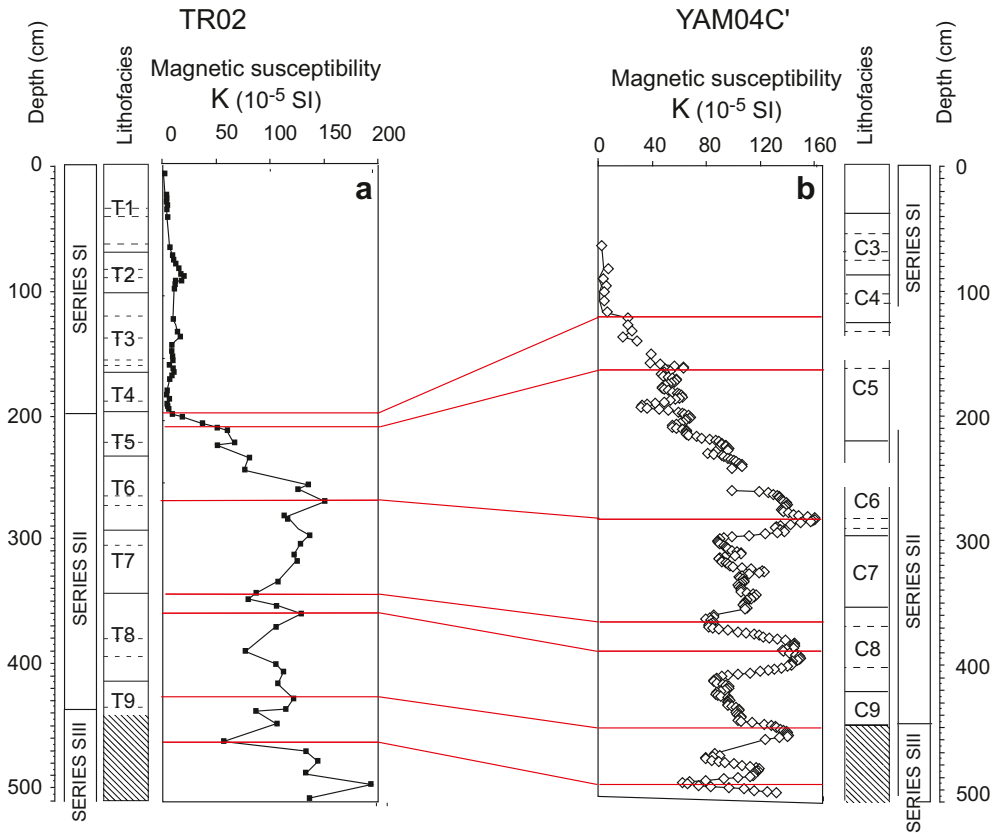

Fig. 8. Magnetic susceptibility (*K*) stratigraphy of the upper 5 m of TR02 (a) and YAM04C′ (b). Red lines, level-to-level correlations based on *K* values.

section (Daëron et al., 2007). Correlation between the core and TR02 can be undoubtedly established between an ash layer (T3d*and C3d*) of similar facies and geochemical composition (Develle et al., 2009) and the underlying layers C3e*-T3e* and C4a-T4a. Units T1 and T2 are apparently missing in the core likely due to tilling. No clear equivalence is found between the lithofacies observed in C5 (112-cm thick) and T5 (25-cm thick), suggesting that unit 5 is partly missing in TR02. The *K* values decrease between 282 and 113 cm in the core is much more progressive than the shift from 264 to 200 cm in the trench, also suggesting a hiatus in unit T5 partially filled up by the core profile. The stratigraphic equivalence of the very dark clay layers of sub-units C6a*-b* and T6a*-b* is based on lithofacies (Fig. 7) and the peak of maximum *K*-values in TR02 and YAM04C′ (Fig. 8).

It is difficult to know from lithology if the waterbody has been permanent at times. Pollen data from the core (E. van Campo, personal communication, 2009) show abundant and well-preserved pollen grains in the lower part of the SI series and C5 top (~166–90 cm), implying a permanent lake because oxidation precludes pollen preservation in a seasonal waterbody. Pollen grains rapidly decrease in number and preservation above and below these depths.

4.2. Chronology

The apparent ^{14}C ages of the four karstic spring water samples from Yammoûneh, range between 1900 and 3900 ^{14}C years before present (BP, Table 1a). A substantial "water reservoir age" in the supplying aquifer is excluded because the residence time in the karstic aquifers of the region is on the order of the year (el Hakim, 2005; Aouad et al., 2005). These ages are attributed to the "hard water effect" (due to dissolution of old limestones) produced by snow-melted water rapidly flowing-down along different subterranean pathways through the Mnaïtra karstic network. This ageing does not affect the stable isotope record supported by ^{14}C ages of terrestrial material. The "hard water effect" on fossil aquatic material is shown by ^{14}C measurements performed on gastropod shells which appear much older than terrestrial remains from the same layer (Table 1b). Therefore material of aquatic origin was discarded for dating purposes.

The ages obtained from wood samples of TR01 (Daëron et al., 2007) and TR02 support the stratigraphic correlations based on lithofacies and allow us to integrate the ages of the very distinctive layers measured in TR01 (Daëron et al., 2007) and in our TR02 chronology (Table 1b). The chronology of the upper 80 cm of TR02

Table 1a
Radiocarbon analyses: radiocarbon activity of total dissolved inorganic carbon in water of karstic springs sampled in September 2004 in the Yammoûneh basin, and corresponding apparent radiocarbon ages.

No. cible	No. IDES	Sample designation	$\delta^{13}C$ pd b	pMC corrected for fractionation	Apparent radiocarbon age (years BP)
SacA 7970	H3426	LIB04 SOU1F	−7.99	78.64 ± 0.33	1930 ± 35
SacA 7971	H3427	LIB04 SOU6F	−7.37	61.64 ± 0.27	3885 ± 35
SacA 7972	H3428	LIB04 SOU2F	−6.57	71.75 ± 0.29	2665 ± 35
SacA 7973	H3429	LIB04 SOU7F	−6.96	70.22 ± 0.27	2840 ± 30

Table 1b
AMS-^{14}C ages of wood fragments and gastropod shells from the sedimentary profiles TR01 (data from Daëron et al., 2007), TR02 and YAM04C′. In bold, ages used for the age model construction of TR02 (Fig. 9). In italic, ages discarded due to ageing by hard water effect (shells) or reworking (core sample).

Stratigraphic profile	Sample	Series	Unit	Depth in TR02 (cm)	Material	Lab ref.	^{14}C age (years BP)	Calibrated age min (2 sigma) (years BP)	Calibrated age max (2 sigma) (years BP)	Calibrated age mean (2 sigma) (years BP)
TR01*	**M-K64**	**SI**	**T1**	**36**	**Wood**	**L-85984**	**1640 ± 45**	**1411**	**1691**	**1551**
TR01*	**M-G5**	**SI**	**T1**	**45**	**Wood**	**G-12236**	**2000 ± 100**	**1714**	**2153**	**1934**
TR02	M162	SI	T2b*	86	Wood	G-12880	5879 ± 50	6634	6750	6689
TR01*	**M-K111**	**SI**	**T2b***	**86**	**Wood**	**L-86077**	**5610 ± 70**	**6283**	**6556**	**6420**
TR01*	M-K13a	SI	T2b*	86	Wood	L-85977	5640 ± 50	6305	6533	6419
TR01*	M-K13a	SI	T2b*	86	Wood	L-85978	5790 ± 45	6478	6719	6599
TR02	*IVIU88788*		*T2b*	*87.05*	*Gastropod shell*	*Beta-245769*	*8010 ± 40*	*9130*	*9420*	*9275*
TR02	**M161**	**SI**	**T2c (base)**	**95**	**Wood**	**G-12881**	**5910 ± 60**	**6660**	**6790**	**6723**
TR02	*IVIU99596*		*T2c (base)*	*95.05*	*Gastropod shell*	*Beta-245770*	*7810 ± 40*	*8990*	*9090*	*9040*
TR02	M157	SI	T3e *	160	Wood	G-12882	8310 ± 60	9132	9465	9299
TR01*	**M-K50b**	**SI**	**T3e* (top)**	**160**	**Wood**	**L-86078**	**8045 ± 45**	**8768**	**9032**	**8900**
TR01*	M-K50	SI	T3e*	160	Wood	L-86066	8405 ± 35	9308	9519	9414
TR01*	**M-K50b**	**SI**	**T3e* (base)**	**163**	**Wood**	**L-85995**	**8250 ± 40**	**9090**	**9403**	**9247**
TR02	**M118**	**SI**	**T4a (base)**	**180**	**Wood**	**G-12904**	**8520 ± 70**	**9331**	**9632**	**9482**
TR01*	**M-K20**	**SI**	**T4c* (top)**	**193**	**Wood**	**L-85981**	**9335 ± 45**	**10414**	**10683**	**10549**
TR01*	M-K129	SI	T4c* (top)	193	Wood	L-86080	9510 ± 70	10587	11100	10844
TR01*	**M-K93**	**SII**	**T5 (top)**	**204**	**Wood**	**L-86076**	**10290 ± 190**	**11389**	**12705**	**12047**
TR02	**M156**	**SII**	**T5b* (base)**	**225**	**Wood**	**G-12905**	**12720 ± 90**	**14635**	**15350**	**14993**
TR02	**M154**	**SII**	**T6a***	**235**	**Wood**	**G-12883**	**16470 ± 130**	**19399**	**19900**	**19650**
YAM04C′	*YAM04C′83*	*SI*	*C3e*	*83*	*Wood*	*Poz-22389*	*9140 ± 50*	*10220*	*10430*	*10325*

is, however, only based on hypothesized correlations between T1 and the top of TR01. In the core, the age measured for unit C3d* appears too old compared to that of unit T3d*-e* in both trenches (Table 1b). No wood fragment was found between 235 and 530 cm in TR02, and between 83 and 533 cm in YAM04C′. Samples deeper than 530 cm are older than 31,000 ^{14}C years BP.

Seventeen AMS-^{14}C ages are available for TR02 (Table 1b). When several ages have been measured for a given stratigraphic level, the youngest age of each group is selected as the closest from the actual age of sedimentation. Indeed, age groups around 6.5 ka and 9.5 ka coincide with remarkable very dark gray or brown clayey-silty, TOM-rich beds of irregular thickness (sub-units T2b* and T3e*; Fig. 7; Supplementary Appendix A), which evoke abrupt surge or erosive events and thus, some reworking. Nevertheless, the age model does not significantly change when taking into account all ages, their mean, or the youngest age of each cluster (not shown). The TR02 age model is finally based on 11 AMS-^{14}C dates (Fig. 9). The apparent mean sedimentation rate is relatively high from ~11 to 6.5 ka. It decreases drastically before ~15 ka likely due to frequent periods of desiccation.

Our chronology confirms the Holocene age of the SI series and allows units T5-C5 and T6-C6 to be assigned to the last deglacial period and to the LGM, respectively. Our age model suffers large uncertainties, however, especially prior to the Holocene period, due to the low number of ^{14}C ages and possible sedimentary hiatus.

4.3. Isotopic composition of water samples

At Yammoûneh, spring and shallow aquifer waters show stable isotopic values (mean: $\delta^{18}O = \sim 8.9‰$, $\delta D = \sim 50.8‰$, $d = 20.5‰$; Table 2) very close to the estimated mean values of local winter rain (Fig. 6d). Water from the pool close to the eastern sinkhole (sample 5, Table 2) is not significantly ^{18}O-enriched compared to spring water, suggesting little evaporative concentration during the water transfer through the plain. The lowest spring water values ($\delta^{18}O = \sim 9.1‰$, $\delta D = \sim 51.7‰$, $d = 21.4‰$) coincides with that of precipitation during the wettest month at Yammoûneh (January) and with the mean winter precipitation values in the western mountain sites (Al Hrazmin, El Aarîch; Fig. 6c). Similar conclusions were drawn from the karstic springs of the Beqaa plain (el Hakim, 2005) and the eastern flank of Mount Lebanon (Aouad et al., 2004, 2005). This indicates that the Yammoûneh aquifer behaves similarly to the nearby aquifers. We conclude that the oxygen isotopic composition of water inflow to the Yammoûneh basin reflects that of winter precipitation in its watershed.

4.4. Isotopic composition of ostracod valves

In the case of $\delta^{18}O$ measured on ostracods, biological factors induce $\delta^{18}O$ differences between individual taxa found in a given water and/or sediment sample. These differences integrate the effects of auto-ecology (microhabitat, seasonality etc.), and the so-called "vital effect", which is the species-dependent difference

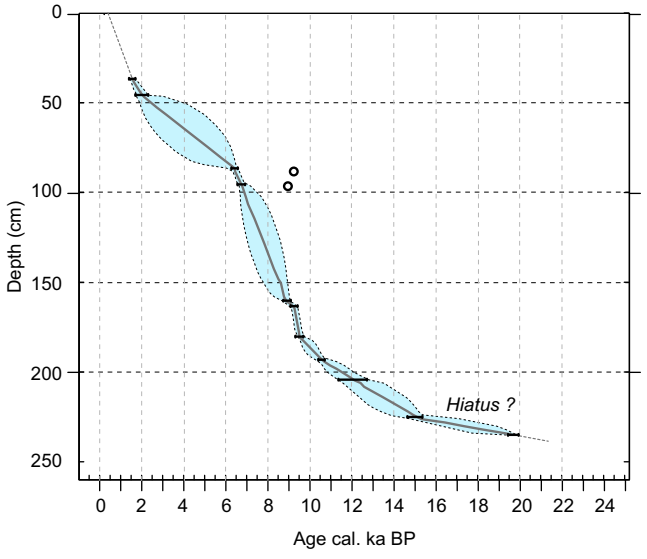

Fig. 9. Calibrated ^{14}C ages versus depth in trench TR02, based on the terrestrial calibration curve IntCal04.14 (Reimer et al., 2005). Error bars on ^{14}C ages: 2σ standard deviation. The dashed curves show maximum age uncertainties as estimated using the Bchron v.2.1 model (Haslett and Parnell, 2008) by calculation of all possible sedimentation rates between two dated points. Circles: ages of gastropod shells biased by dead carbon in the TDIC of karstic water supplying the lake.

Table 2
Isotopic composition ($\delta^{18}O$, δD, $d = \delta D - 8 \times \delta^{18}O$, ‰ vs. SMOW) of water collected in September 2004 in the Yammoûneh basin from: (1–4) karstic springs; (5) a small pool close to an eastern sinkhole; (6) aquifer level crossed at 21 m depth during coring. Analyses performed by C. Vallet-Coulomb, CEREGE, Aix-en-Provence.

Sample type	Sampling date	Sample designation	$\delta^{18}O$ (‰ vs. SMOW)	δD (‰ vs. SMOW)	Deuterium excess (‰ vs. SMOW)	Temperature (°C)	pH
1	Sept. 2004	LIB04 SOU1F	−9.04	−52.3	20.02	11	8.03
2	Sept. 2004	LIB04 SOU2F	−9.14	−51.7	21.42	11	8.11
3	Sept. 2004	LIB04 SOU6F	−9.03	−52	20.24	10	8.18
4	Sept. 2004	LIB04 SOU7F	−8.7	−48	21.6	11.5	8.11
5	Oct. 2004	LIB04 pool	−8.77	−51.3	18.86		
6	Sept. 2004	YAM04C aquifer (−22 m)	−8.7	−50	19.6		
		Mean	−8.94	−51.06	20.428		

between the shell isotopic composition (δ_{ost}) and that of inorganic calcite (δ_c) precipitated in isotopic equilibrium with the ambient water (e.g., Xia et al., 1997a,b; von Grafenstein et al., 1992, 1999; see a detailed discussion in Schwalb, 2003). A number of culturing experiments, field works and fossil records show a systematic $\delta_{ost} - \delta_c$ difference in adults of a given ostracod taxon, indicating that the vital offset is constant with time and environmental conditions. All the data measured in this study are shown in Table 3, but only the $\delta^{18}O$ values will be considered in the following since our purpose focuses on the oxygen isotopic composition of the lake water.

4.4.1. Interspecies $\delta^{18}O$ differences

Two sets of samples where *I. gibba* and/or *C. neglecta* co-occur with *I. inermis* in the Yammoûneh sediments were analyzed for their $\delta^{18}O$ (δ_{ost}) to determine interspecies differences ($\Delta\delta^{18}O_{sp}$) (Table 3). These differences integrate the species-specific vital offset and the effects of auto-ecology. Note that, in our case study, sediment samples (1-cm thick minimum) represent at least 2–3 decades and that environmental variability at shorter time scales is blurred.

Oxygen isotopic composition measured in 13 samples containing adult *I. inermis* and *I. gibba* show a mean $\Delta\delta^{18}O_{sp}$ of 0.01 ± 0.21‰ (Table 3). This negligible difference suggests that the two taxa lived under the same ecological conditions and had a similar vital offset, or that different species-specific signatures are counterbalanced by seasonal temperature fluctuations. Conversely, a significant isotopic difference appears between *C. neglecta* (juvenile) and *I. inermis* from five samples containing both taxa with a $\Delta\delta^{18}O_{sp}$ of -0.18 ± 0.16‰. Both *I. inermis* and juvenile *C. neglecta* likely occurred all year round in the Holocene lake, suggesting that $\Delta\delta^{18}O_{sp}$ reflects different vital effects. It is noteworthy to mention that the standard deviation calculated for the $\Delta\delta^{18}O_{sp}$ values represents less than 10% of the total variations of the composite $\delta^{18}O$ record and will therefore not alter the interpretation of the isotope record (Fig. 10).

4.4.2. Estimate of the $\delta^{18}O$ calcite (δ_c)

It is commonly accepted that the vital effect is similar for different species of a given genus, or even of a given family (von Grafenstein et al., 1999). However, Belis and Ariztegui (2004) have compared $\delta^{18}O_{ost}$ values between *C. neglecta* and *Ilyocypris bradyi* in Lake Albano (Italy), and found a difference, $\Delta\delta^{18}O_{I.\ bradyi\ -\ C.\ neglecta}$, of −1.5‰, larger than that observed between our specimens of *I. inermis* and *C. neglecta* (−0.18‰). This suggests a species-specific geochemical signature, or a large range of habitats for different *Ilyocypris* species, which cannot be detected in our case study. Although it was suggested, on the basis of a limited data set from Lake Issyk-Kul (Kazakhstan), that $\delta^{18}O$ of *C. candida* may be up to 0.3‰ more positive than *C. neglecta* (Park et al., 2003), no significant difference between members of the *Candona* clade has been noted by other workers. The "vital effect" of Candoninae has been

Table 3
$\delta^{18}O$ and $\delta^{13}C$ differences between *Ilyocypris inermis* (here regarded as the reference taxon) and the two other species abundant in the sedimentary sequences, *Ilyocypris gibba* and *Candona neglecta*. SD, standard deviation.

Species	Depth (cm)	$\delta^{18}O_{I.\ gibba}$ (‰ PDB)	$\delta^{13}C_{I.\ gibba}$ (‰ PDB)	$\delta^{18}O_{I.\ inermis}$ (‰ PDB)	$\delta^{13}C_{I.\ inermis}$ (‰ PDB)	$\Delta\delta^{18}O$ ($\delta^{18}O_{I.\ inermis} - \delta^{18}O_{I.\ gibba}$) (‰ PDB)	Mean	SD (1 sigma)	$\Delta\delta^{13}C$ ($\delta^{13}C_{I.\ inermis} - \delta^{13}C_{I.\ gibba}$) (‰ PDB)	Mean	SD (1 sigma)
I. gibba	15.5	−6.92	−6.88	−6.99	−6.86	0.06			0.02		
	120.5	−7.52	−6.42	−7.59	−6.35	0.07			0.07		
	150.5	−7.56	−6.07	−7.71	−6.20	0.15			−0.13		
	286	−5.96	−6.04	−5.93	−5.74	−0.03			0.30		
	293.5	−5.70	−4.94	−5.95	−6.11	0.25			−1.17		
	305	−6.56	−6.41	−6.56	−6.70	0.00			−0.29		
	310	−6.35	−6.65	−6.13	−6.76	−0.22			−0.11		
	315	−6.27	−7.00	−6.45	−7.06	0.18			−0.06		
	320	−6.57	−6.74	−6.27	−6.80	−0.30			−0.06		
	324	−5.84	−6.70	−5.74	−6.48	−0.10			0.22		
	332	−6.35	−7.29	−6.06	−7.19	−0.28			0.10		
	339.5	−6.31	−7.08	−6.30	−7.31	−0.02			−0.23		
	344	−6.32	−7.28	−6.72	−7.50	0.40			−0.22		
							0.01	**0.21**		**−0.12**	**0.36**
		$\delta^{18}O_{C.\ neglecta}$ (‰ PDB)	$\delta^{13}C_{C.\ neglecta}$ (‰ PDB)	$\delta^{18}O_{I.\ inermis}$ (‰ PDB)	$\delta^{13}C_{I.\ inermis}$ (‰ PDB)	$\Delta\delta^{18}O$ ($\delta^{18}O_{I.\ inermis} - \delta^{18}O_{C.\ neglecta}$) (‰ PDB)	Mean	SD (1 sigma)	$\Delta\delta^{13}C$ ($\delta^{13}C_{I.\ inermis} - \delta^{13}C_{C.\ neglecta}$) (‰ PDB)	Mean	SD (1 sigma)
C. neglecta	15.5	−7.07	−4.95	−6.99	−6.86	0.09			−1.91		
	50.5	−6.47	−4.99	−6.72	−6.77	−0.25			−1.78		
	120.5	−7.38	−4.28	−7.59	−6.35	−0.20			−2.07		
	145.5	−7.14	−4.58	−7.49	−5.57	−0.35			−0.99		
	150.5	−7.52	−3.96	−7.71	−6.20	−0.19			−2.24		
							−0.18	**0.16**		**−1.80**	**0.48**

estimated (from a 1-year monitoring in two German lakes) to be about +2.2 ± 0.15‰ including small differences between different juvenile stages (von Grafenstein et al., 1999). Assuming a mean vital effect of +2.2‰ for our specimens of *C. neglecta*, we estimate the vital effect of *I. inermis* at +2.4 ± 0.2‰, taking into account the $\delta^{18}O$ difference found in our samples (Table 3).

These observations allow us to construct a single isotope record for each sedimentary profile (Fig. 10a). All $\delta^{18}O_{ost}$ values were normalized to *I. inermis* (−0.18‰ correction for *C. neglecta* and no correction for *I. gibba*), and then corrected by +2.4‰ (the estimated average of the *I. inermis* vital effect) to obtain $\delta^{18}O$ values coeval with theoretical $\delta^{18}O$ of inorganic calcite in equilibrium with lake water. The isotope records show two major phases broadly corresponding to the stratigraphic series SI and SII, with higher values in the Late Pleistocene layers (SII) than in the Holocene deposits (SI). The highest δ_c values are observed at 227 cm (−7.93‰) in TR02 and at 216 cm (−8.09‰) in the core (units T5-C5) (Figs. 10a). Above these depths, δ_c markedly decreases to reach almost similar values of −9.3‰ at 200 cm in TR02 and −9.2‰ at 182 cm in the core. Sharp positive excursions occur at 191.5 cm in TR02 (−8.4‰), and at 133 (8.1‰) and 120 cm (8.4‰) in the core. The most depleted δ_c values (−10.1 to −10.3‰) are observed at 170–150 cm in TR02 and at 90–70 cm in the core (units T4a-C4a top, T3c-C3d). Above, the trench profile records a progressive isotopic enrichment up to about −9‰.

4.4.3. Trench to core correlation and construction of a composite δ_c profile

Similarities in the isotopic features of the TR02 and YAM04C′ profiles (Fig. 10a) suggest stratigraphic correlations in overall agreement with those proposed from lithofacies (Fig. 7) and magnetic susceptibility (Fig. 8). Using marker beds defined from the 3 proxies established independently (Table 4), a composite isotope profile as a function of depth was constructed by linear interpolations (Fig. 10b). We have chosen an arbitrary depth scale based on TR02 (0 cm at the trench top). Below the uppermost correlation points (145.5 cm in TR02, 63 cm in the core), the depth difference between these two points (82.5 cm) was applied to all core samples to adjust the two profiles versus trench depth.

The chronology established for TR02 (Table 1b; Fig. 9) was then integrated to the core section, providing a composite δ_c profile as a function of age for the ^{14}C-dated part of the sequence (Fig. 11). According to our age model, high δ_c values characterize the interval ~22–19 ka (LGM). The lack of ostracod data from ~19–15.5 ka coincides with a period of extremely low mean sedimentation rate (Fig. 9) suggesting droughts during the early stages of the last deglaciation. A negative shift took place from ~15.5 to ~13.4 ka (the Bölling-Alleröd period). From 13.4 to 11.5 ka, δ_c increased but did not show the high values of two subsequent peaks dated at ~11.1 and 10.6 ka (earliest Holocene). The δ_c values reached their minimum (~2.5% lower than LGM values) between ~9.5 and 8.5 ka and remained low until ~7 ka. Then, δ_c steadily increased during the mid–late Holocene.

Over the past 12 ka, similar trends between our δ_c record and that from the nearby U/Th dated Jeita Cave speleothem, located at ~100 m.a.s.l. near Beirut at ~5 km from the coast line (Figs. 1 and 2), gives confidence to our chronology. In particular, the Jeita record also shows marked positive peaks at the onset of the Holocene, which apparently lag the YD chronozone (Fig. 11). Prior to the Holocene

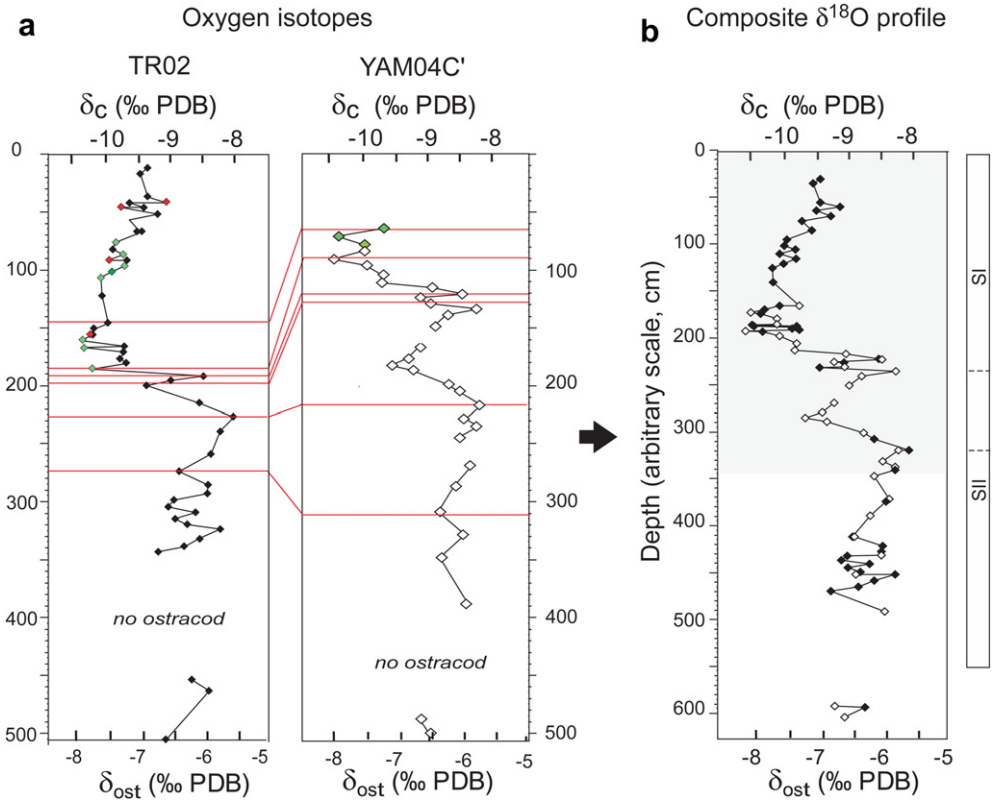

Fig. 10. The Yammoûneh oxygen isotope record. (a) Ostracod $\delta^{18}O$ values (δ_{ost}), all normalized to *Ilyocypris inermis*, in TR02 and YAM04C′, shifted to δ_c (coeval with theoretical $\delta^{18}O$ of inorganic calcite) by correction for the specific vital effect. Red and green symbols correspond to values obtained on *Candona neglecta* and on *I. gibba*, respectively, in samples devoid of *I. inermis*. Red lines, trench to core stratigraphic correlations based on $\delta^{18}O$ values. (b) Construction of a composite $\delta^{18}O_{ost}/\delta^{18}O_c$ profile as a function of depth, based on level-to-level correlations derived from $\delta^{18}O$ values (a), lithofacies (see Fig. 7 and Supplementary Appendix A) and total magnetic susceptibility (see Fig. 8). Black and white dots, TR02 YAM04C′ samples, respectively. The depth scale is arbitrarily chosen with 0 cm for the trench top). In the text, the discussion only concerns the ^{14}C-dated part of the profile (pale gray rectangle shown in (c).

Table 4
Depth of the marker beds identified from lithofacies (Fig. 7, Supplementary Appendix A), magnetic susceptibility (Fig. 8) and ostracod $\delta^{18}O$ (Fig. 10) in the trench TR02 and core YAM04C′, and used for the stratigraphic correlation between the two profiles.

Proxies	Depth TR02 (cm)	Corresponding depth in YAM04C′ (cm)
Lithofacies	155	70
	160	83
	200	133
	268	295
Magnetic susceptibility	197	125
	206	166
	264.8	282
	343	364
	355	392
	423	456
	457	492
Oxygen isotopes ostracods	145.5	63
	185.5	90
	191.5	120
	199.5	128
	215	204
	227	216
	274	308

period, the strict timing of specific events may be subject to change with an improved chronology.

5. Discussion

5.1. Significance of the oxygen isotopic composition of lake and speleothem carbonates

The oxygen isotope composition of carbonate that precipitated in equilibrium with an aqueous solution is controlled by the temperature of the ambient water and its isotopic composition. In inland systems such as lakes and caves, these two major controls depend on both climate and site-specific factors.

5.1.1. Temperature dependence

The temperature dependence between the $\delta^{18}O$ content of calcite that precipitates in equilibrium with the ambient water, δ_c, can be expressed by one of the "paleotemperature" equations, e.g., Craig and Gordon, 1965:

$$T_{water} = 16.9 - 4.2(\delta_c - \delta_{water}) + 0.13(\delta_c - \delta_{water})^2 \quad (1)$$

where T_{water} (°C) is the water temperature at the time of precipitation, δ_c is the $\delta^{18}O$ content of the carbonate expressed in ‰ vs. PDB, and δ_{water} is that of the ambient water expressed in ‰ vs. SMOW. The δ_c value decreases by ~0.22 ‰ per 1 °C increase in water temperature. Such an equation is valid for carbonate precipitating in lake water (δ_L), cave water ($\delta_{cave\ water}$), and sea waters (δ_{sw}).

5.1.2. Isotopic composition of ambient water

In a lake, the water isotopic composition depends on the lake water balance and the isotopic composition of its components. For thorough investigation of stable isotopes in lake water, we refer to fundamental works, e.g., Craig and Gordon (1965), Gonfiantini (1986), Gat (1995). The $\delta^{18}O$ balance of a lake during the time dt is given by:

$$d(V \cdot \delta_L V)/dt = I\delta_I - Q\delta_Q - E\delta_E \quad (2)$$

where V is the volume of the lake water having a mean isotopic composition δ_L, I, Q and E are the fluxes of inflows (precipitation on the lake surface + surface runoff + groundwater discharges), Q includes river and bottom infiltration, and E evaporation flux from the lake surface, respectively; δ_I, δ_Q and δ_E are the respective weighted mean isotopic compositions.

The water inflow (I) is governed by regional rainfall amount (P) modified by evaporation, evapotranspiration and infiltration in the watershed. The $\delta^{18}O$ of the inflowing water (δ_I) reflects the rainfall $\delta^{18}O$ (δ_P) enriched through evaporation. Whatever the system, the initial control of δ_P (and thus of δ_I) is the isotopic composition of the water vapor source area (in our case, the EM surface water), and its evolution along the air mass trajectory and during condensation (including continentality, altitude, temperature, rainfall amount effects; Dansgaard, 1964; Rozanski et al., 1993). The term Q is closely linked to the lake basin morphology and to the lake bottom permeability. If the lake is well mixed, $\delta_Q = \delta_L$. The evaporation flux, E, is a function of the lake surface area, relative air humidity and

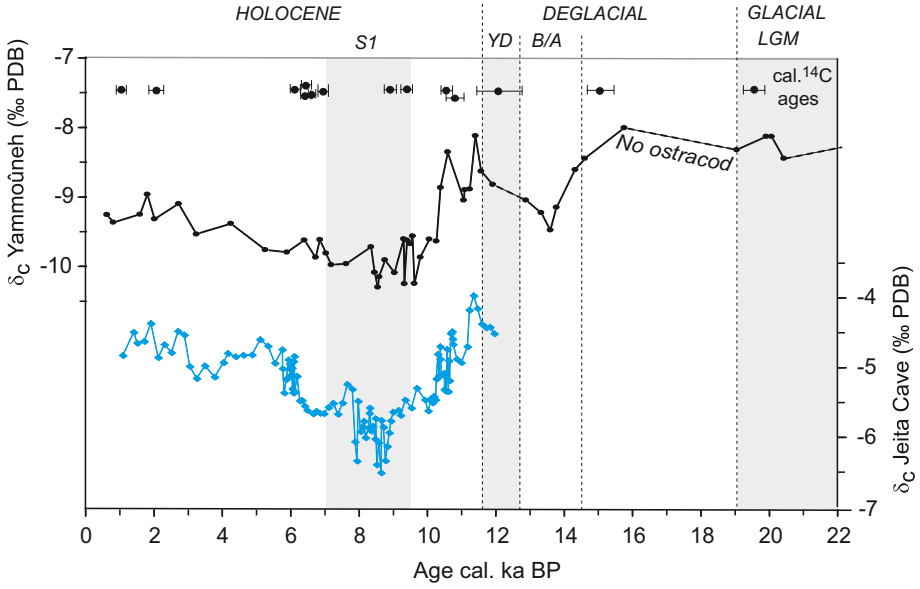

Fig. 11. Comparison of the δ_c profiles from Lake Yammoûneh (this work) and from the Jeita Cave speleothem (Nader et al., 2007; Verheyden et al., 2008) as a function of ages. Calibrated ^{14}C dates (2σ standard deviation uncertainty) from Yammoûneh are shown. Specific time intervals as for Fig. 2.

wind stress, and induces enrichment in heavy isotopes ($\delta_E < \delta_L$). According to Craig and Gordon (1965), δ_E also depends on climate variables, namely relative air humidity, isotopic composition of air moisture above the lake (that generally tracks δ_p), and thermodependent equilibrium fractionation and enrichment factors.

At hydrological steady state (no change in lake volume) and assuming that other variables remain unchanged during the time interval considered, δ_L reaches a steady-state value with time. Climate changes lead to transient conditions from one steady state to another. The longer the water residence time (V/I or $V/[Q+E]$), the longer is the time required to reach isotopic steady-state. Differences in the long-term behavior of lakes subjected to the same climatic forcing but with different water balance were clearly illustrated in the review of $\delta^{18}O$ records from Mediterranean lakes over the past 20 ka (Roberts et al., 2008). Closed lakes ($Q = 0$; e.g., the Dead Sea) generally exhibit high δ_L values compared to δ_I due to evaporative concentration. These lakes show large δ_c fluctuations and are good recorders of long-term changes in the isotopic composition of the source (Kolodny et al., 2005) and in regional hydrological balance (P-E) which override the effects of temperature changes (Roberts et al., 2008). In contrast, δ_L remains closer to δ_I in open lakes, where long-term δ_L and δ_c fluctuations are moderate. Unfortunately, few works have been performed on long-term changes in open lakes from the Levant. The last glacial–Holocene record in Lake Huleh (Stiller and Hutchinson, 1980), which suffers dating uncertainties (Roberts et al., 2008), shows δ_c variations of a few ‰. The Kinneret record (Stiller and Kaufman, 1985; Dubowski et al., 2003) only covers the past 5.5 ka. In small open lakes with extremely rapid through flow, E is very small or negligible, and δ_L is very close to δ_I. If δ_I is not significantly modified compared to rain value, δ_L represents the average isotopic composition of precipitation in the lake catchment, and δ_c can be used as a proxy indicator of the composition of regional rainfall and of water temperature (Siegenthaler and Eicher, 1986; Talbot, 1990; Leng and Marshall, 2004).

In a cave, the water inflow and its isotope composition before infiltration, I and δ_I, have the same significance as for a lake system. The speleothem δ_c value is primarily related to the $\delta^{18}O$ value of drip water ($\delta_{cave\ water}$) and to the cave temperature. The drip water $\delta^{18}O$; value is modified compared to δ_I by complex site-specific processes in the soil zone and the epikarst. These modifications remain, however, relatively moderate when compared, for example, to the impact of evaporation in a closed lake. The cave temperature is generally representative of the mean annual ground temperature (MAT) above the cave. For further details, we refer to comprehensive reviews on $\delta^{18}O$ in speleothem carbonates (e.g., Lachniet, 2009).

5.1.3. The case of the Yammoûneh lake

The lake at Yammoûneh was small and shallow, and thus assumed to be well mixed. It was subject to important water losses by leakage through its permeable lake bottom. At least since Roman times, it was a seasonal lake only filled during the time of snow melting and maximum karstic spring discharge. It was likely permanent during the early–mid Holocene. Although evaporation has certainly acted on the lake $\delta^{18}O$ balance, its role is believed to have been extremely reduced because: (i) no signal of evaporative salt concentration is observed, neither from lithofacies nor biological remains (except, may be, during intervals where the ostracod *I. gibba*, which tolerates slightly saline waters, developed; Fig. 10); (ii) the range of δ_c fluctuations along the profile is small; and (iii) when the lake was ephemeral, it was dry during the warmest, driest season. Modern data show that the isotopic composition of the water inflow to the basin, δ_I, is representative of the winter rainfall isotopic composition in the whole catchment which is close to the isotopic annual weighted mean, δ_P ($\delta_I \approx \delta_P \approx 8.9$‰; Table 2, Fig. 6). We thus consider the Yammoûneh paleo-lake as a small open lake with fast discharge and low evaporative enrichment where δ_L approximates δ_I and δ_P, and where δ_c is primarily sensitive to changes in the isotope composition of precipitation and in water temperature.

Over a hydrological cycle, the water temperature in such a small lake is believed to rapidly equilibrate with air temperature, although the karstic spring water (mean annual temperature: 7.5 °C with minor seasonal changes; Hakim, 1985) should have partly dampened the seasonal air temperature variations. When the lake was seasonal, δ_c values were related to the temperature of March–early July, when the lake existed and ostracods grew. The mean air temperature of these months is close to the annual mean today (Fig. 4). When the lake was permanent, we assume that δ_c values corresponded to the mean annual temperature (MAT) because the ostracod taxa here analyzed are found all year round in modern waterbodies. Since we have no means to constrain past seasonality changes, we will only refer in the following discussion to mean annual temperature and precipitation changes.

In order to explore the significance of our Yammoûneh isotopic record, we first tentatively correct the δ_c signal for water temperature to obtain the paleo-lake water isotopic composition, and as a second step correct the signal for the Mediterranean "source effect". Because δ_c values in speleothems are also closely related to temperature and δ_I, the same approach is conducted on the speleothem δ_c records from Jeita and Soreq Caves for comparison. Common trends and differences between sites allow us to discuss qualitatively (and with a series of assumptions) the relative role of changes in regional versus more local, site-specific factors acting on terrestrial environments.

5.2. Correction of inland δ_c records for water temperature

Regional temperature changes may have affected the terrestrial δ_c records in two ways: (i) through the temperature of water (where the carbonates precipitate), and (ii) through the isotopic composition of inland precipitation ("ground-temperature effect"). Here, we attempt to evaluate the effect of the water temperature.

5.2.1. Reconstruction of the Yammoûneh lake water isotopic composition, δ_L

Since no local paleotemperature reconstruction is available, we have considered regional temperature estimates. Inland, a mean annual temperature difference relative to modern (ΔT) of ~6 °C has been empirically estimated for the LGM (Horowitz, 1979) from pollen data of central Israel. Improved statistical techniques applied to pollen data yield an LGM ΔT of $\sim 11 \pm 3$ °C at Ghab (southern Syria; Wu et al., 2007), and to an area-averaged time series MAT reconstruction for the past 12 ka in the region around the eastern Mediterranean (Davis et al., 2003). Land temperatures were also obtained using geochemical methods on the speleothem carbonate material of Soreq Cave, i.e., δD analyses of fluid inclusions associated with the $\delta D - \delta^{18}O$ of carbonate relationship and the carbonate paleotemperature scale (McGarry et al., 2004), and "clumped isotope" thermometry (Affek et al., 2008). Results from these methods suggest inland ΔTs ranging from ~6 to ~11 °C from 19 to 22 ka (LGM). On the other hand, Bar-Matthews et al. (2003) have suggested that alkenone-derived sea surface temperatures (SST_{alk}) in the Levantine basin can be used as a proxy for land MATs. Available SST_{alk} records from the Levantine basin (Emeis et al., 2000, 2003; Essallami et al., 2007; Almogi-Labin et al., in press) indicate LGM ΔT values of ~6 to ~10 °C. Although LGM SSTs inferred from planktonic foraminifera assemblages using the modern analogue technique have suggested a ΔT of −1 to −3 °C only (Hayes et al., 2005) for the EM, this estimate is discarded because the insufficient

number of close modern analogues makes this technique unreliable in the region prior to ~13 ka (Essallami et al., 2007).

Any technique for reconstructing paleotemperature has its own source of uncertainties, and significant discrepancies appear between the different reconstructions due to local factors, different time resolution of the records, or those inherent to the proxy and technique used. Nevertheless, all reconstructions indicate a cooling of ~6 to ≥−10 °C during the LGM, and early–mid Holocene temperatures close to or slightly lower than modern.

In order to reconstruct δ_L, we have considered "land" paleotemperature records. However, because of the lack of "land" data for the time interval 12–18 ka, we also took into account the SST_{alk} record from core MD84-632 (Essallami et al., 2007), which is to date the most continuous and best resolved EM SST_{alk} record and which shows a cooling of 6–7 °C for the LGM compared to the mid Holocene (21 °C). We have plotted the difference from modern SST (22.4 °C, Levitus and Boyer, 1994). The temperature anomalies compared to modern (ΔT) used in this study are shown in Fig. 12a. When several temperature values were available, the mean and the range were considered. All temperature data corresponding to our δ_c record were interpolated. We then applied the paleotemperature equation (Eq. (1)) to obtain the lake water isotopic composition, δ_L (mean and range; Fig. 12b). In our reconstruction, we assume that the differences observed today between mean annual temperature at Yammoûneh (MAT: 15 °C), Soreq Cave (MAT: 18 °C, Bar-Matthews et al., 1997), and the marine site (SST: 22.4 °C) remained constant through time. This is a very crude assumption as the LGM altitudinal thermal gradient was probably steeper than today (Farrera et al., 1999; Kuhlemann et al., 2008). This point is discussed later.

We are aware that our δ_L reconstruction suffers very large uncertainties due to: (i) uncertainties on our chronology; (ii) the wide range of ΔT estimates; (iii) the assumption of a constant thermal difference between sites, and (iv) the assumption that the Yammoûneh isotope signal is related to MAT rather than to seasonal changes. However, major trends and differences from modern, if not representing absolute values, can be regarded as significant at least for the LGM and the early Holocene when ages and ΔTs are relatively well constrained.

The $\delta^{18}O$ values of the paleo-lake water, δ_L, are regarded here as close to that of its water inflow and as a surrogate indicator of rainfall $\delta^{18}O$ in the catchment, δ_P. The difference between the isotopic composition of the modern water inflow, δ_I, and past δ_L values reaches maximum amplitude around 9.5–8 ka (early Holocene; $\sim -2 \pm 0.5‰$) and ~19–21 ka (LGM; $-2 \pm 1‰$) while δ_L values close to modern δ_I are observed around 11–12 ka and after 2.5 ka (Fig. 12b).

5.2.2. Reconstruction of cave water isotopic composition

Using the same approach as for Yammoûneh for the calcite $\delta^{18}O$ records of speleothems from Jeita and Soreq Caves, we can estimate the isotopic composition of the cave water ($\delta_{cave\ water}$). Note that the past Soreq $\delta_{cave\ water}$ has already been reconstructed by using old land paleotemperature estimates (Bar-Matthews et al., 1997) or the Emeis et al. (2000) SST_{alk} data from site ODP 967 (Bar-Matthews et al., 2003). The later led to reconstructions of paleorainfall $\delta^{18}O$ values and amounts for the past 16 ka which suggests a marked YD drought (Bar-Matthews et al., 2003). The Emeis et al. (2000) SST-series has then been reassessed and the up-to-date data file (Emeis et al., 2003; K. Emeis, personal communication, 2008) has a very low time resolution for the time interval here considered (except for the early–mid Holocene) and does not show any YD cooling, in contrast with Emeis et al. (2000). Here, we use the ΔT data plotted in Fig. 12a with the same reserves as for Yammoûneh.

At Jeita, the modern cave temperature is 22 °C (Nader et al., 2007) but the modern isotopic composition of the cave water is unknown. Assuming that, for the past 1.5 ka, δ_c values are representative of modern conditions and using Eq. (1) (with $T = 22 \pm 1$ °C), the isotopic composition of the cave water is about $-3.4 \pm 0.3‰$. This value corresponds to that of the winter rain water at the closest station (Shaileh, $\delta^{18}O \sim -5.4‰$; Fig. 5) enriched by about 2‰ by evaporation in the watershed and mixing processes in

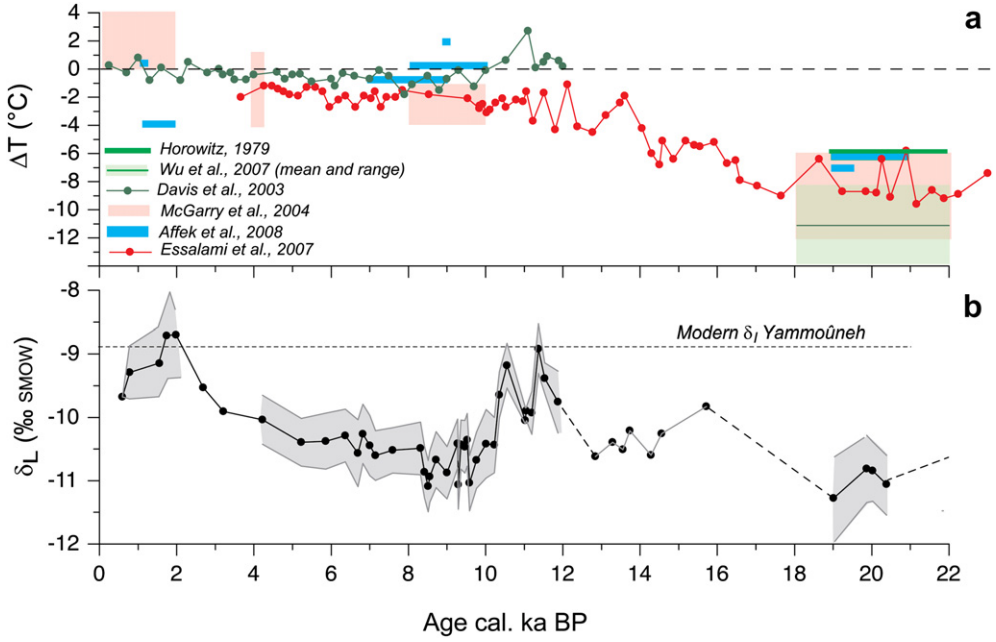

Fig. 12. Tentative correction of the Yammoûneh carbonate $\delta^{18}O$ profile (δ_c) for water temperature. (a) Temperature anomalies relative to modern (ΔT °C), derived from: (i) pollen data (green) from central Israel (after Horowitz, 1979), the Ghab valley (Wu et al. (2007), and SE Europe–eastern Mediterranean region (Davis et al., 2003); (ii) Soreq Cave speleothem δD of fluid inclusions (pink, McGarry et al., 2004) and Δ47 (blue, Affek et al., 2008). (iii) alkenone-derived sea surface temperatures (SSTs) from MD84-632 (red, Essallami et al., 2007). (b) Estimates of the oxygen isotope composition of the Yammoûneh lake water, δ_L, after correction of δ_c for temperature. The black line and the gray surface represent the mean and range of δ_L reconstructions based on all ΔT estimates.

the unsaturated zone. At Soreq, the modern cave temperature is 18–22 °C (Bar-Matthews et al., 1997), and cave water ($\delta^{18}O \sim 5‰$) is approximately 1.3‰ enriched relative to the concurrent rainfall (annual weighted mean $\delta^{18}O \sim 6.3‰$) (Bar-Matthews et al., 2003).

Our δ_L and $\delta_{cave\ water}$ reconstructions are reported in Fig. 13 (mean values; uncertainties are close to those at Yammoûneh, Fig. 12b). As for modern δ_P (or inflow water) values, increased "altitude" and "continentality" effects appear from the lowest site close to the seashore (Jeita), to the Yammoûneh basin lying in altitude on the eastern flank of Mount Lebanon. All reconstructions show changes in the range of 2–2.5‰. Compared to the modern inflows, all exhibit strongly depleted values during the early–mid Holocene, and values close to modern around 12 ka and during the late Holocene. Conversely, during the LGM, δ_L values at Yammoûneh are much lower than δ_I while the $\delta_{cave\ water}$ at Soreq Cave seems to be close to modern.

5.3. The "source effect" on $\delta^{18}O$ of inland water

By considering the overall similarities in shape and amplitude of changes in land and marine δ_c records, it appears that, at long-term time scales, the "source effect" has likely been the main control on the terrestrial isotopic records (e.g., Frumkin et al., 1999; Kolodny et al., 2005). In the following we go one step further by correcting our δ_L and $\delta_{cave\ water}$ signals for this primary control, in order to explore second order factors. Temporal changes in EM sea surface water isotopic composition, δ_{sw}, were estimated by combining the foraminiferal $\delta^{18}O$ values and SST_{alk} data (using Eq. (1)) from core MD84-632 (Essallami et al., 2007) (Fig. 13a). The same general trend is obtained when using the data from core ODP 967, with however lower temporal resolution (Emeis et al., 2003; data not shown).

The marine δ_{sw} was then substracted from the inland water values (δ_L or $\delta_{cave\ water}$) from each site. All time series were resampled at 500-year intervals from 0 to 12 ka, and at 1000-year intervals for older periods. The differences between marine and terrestrial water composition $[\Delta(\delta_L - (\delta_{sw})]$ or $[\Delta(\delta_{cave\ water} - (\delta_{sw})]$ were normalized to the modern difference between δ_I or $\delta_{cave\ water}$ and δ_{sw} values (Figs. 13e). While this difference is low at all three sites during the Holocene period, it appears much larger at Yammoûneh than at Soreq during the LGM (even when taking uncertainties into account), implying that additional factors have to be considered to explain the hydrological evolution at Yammoûneh. Some of these factors are suggested below.

5.4. The major time intervals

5.4.1. The Holocene period

Over the past 11.5 ka, the terrestrial δ_L and $\delta_{cave\ water}$ records covary and run roughly parallel to the EM δ_{sw} record (Figs. 13a–d). This suggests that the three inland sites were influenced by similar climatic trends and that the "source effect" has been a major control on inland precipitation isotopic composition. The two sites from Lebanon are however characterized by two narrow positive $\delta^{18}O$ peaks at the onset of the Holocene not found in the other records. The first peak at ~11.1 ka might reflect the end of a YD event when ΔT is possibly overestimated, while the second one at 10.6 ka suggests a local abrupt event. Nevertheless, the most striking feature shown in Fig. 13 is the almost nil difference $\Delta(\delta_{inland\ water} - \delta_{sw})$ between about 10 and 7–6 ka (Fig. 13e) when all inland sites exhibit their minimum $\delta^{18}O$ values (Figs. 13b–d). This clearly shows that the negative δ_{sw} shift has largely contributed to the early–mid Holocene ^{18}O-depletion of inland water. This time interval broadly coincides with the deposition of sapropel SI in the EM basin (Röhling, 1994; Emeis et al., 2003) when deep EM waters became anoxic in response to increases in freshwater influx and primary productivity (Röhling, 1994). One source of increased freshwater influx to the EM has been the Nile River discharge (Fontugne et al., 1994; Almogi-Labin et al., in press), but stronger precipitation on the Mediterranean Sea may have also contributed to the freshening of the surface marine water (Kallel et al., 1997). Lake records from the whole Mediterranean region also suggest increased inland precipitation at that time (Roberts et al., 2008). The later hypothesis can hardly be tested from $\delta^{18}O$ values alone, but is strongly supported by other proxies from Lebanon. At Jeita, low $\delta^{13}C_{carbonate}$ values, indicator of soil CO_2 concentration and thus of vegetation cover, suggest conditions wetter than modern from ~11.5 to 5.9 ka (Verheyden et al., 2008). Pollen data show that deciduous oak forests reflecting wet, warm conditions were developed from 10.1 to 6 ka around the Aammiq marsh in the Beqaa valley (Hajar et al., 2008), and from >12 to 8.6 ka at Yammoûneh (E. van Campo, personal communication, 2009). In summary, we attribute the Holocene $\delta^{18}O$ fluctuations in inland water from the northern Levant to the primary effect of the source isotope composition (EM δ_{SW}) amplified by increased inland rainfall during the early Holocene.

This conclusion broadly agrees with the interpretation of the Holocene speleothem record from Soreq Cave (Bar-Matthews et al., 2003) where early Holocene relative air humidity much higher than during the late Holocene (70% vs. 45%) has been recently suggested (Affek et al., 2008). In the southern Levant, the Dead Sea level reconstruction also indicates wet conditions relative to modern during the early Holocene (Migowski et al., 2006, Fig. 2a), but the timing of subsequent rapid climate changes seems to be quite different from the northern Levant. The Lebanese records do not reveal the drastic drought around 8 ka observed southward, and, according to the Jeita and Aammiq marsh records, the major shift from humid to dry conditions may have occurred around 6 ka, sooner than in the Dead Sea.

5.4.2. The Lateglacial period

Little can be said for the time interval 19–12 ka because our chronology and ΔT estimates (only based on one SST record) are both poorly constrained, and because our ostracod record is discontinuous. The δ_{sw} values were generally higher than modern but their moderate decrease after 16 ka has probably affected the isotopic composition of inland water. However, this decrease alone can hardly explain the drastic shift in the $\Delta(\delta_{inland\ water} - \delta_{sw})$ difference observed at Yammoûneh and Soreq Cave during the B/A period. At that time, pollen records from the northern Levant indicate enhanced rainfall (Yasuda et al., 2000; Hajar et al., 2008), while most authors record aridification in the Dead Sea–Lisan basin (Fig. 2a). At Yammoûneh, a warming/wetting initiated around 15.5 ka and increased sharply after 13.4 ka. The beginning and end of the YD are characterized by high frequencies of tree pollen taxa which reflect wet warm conditions (E. van Campo, personal communication, 2009). This fact might agree with a wet YD climate as recently proposed for the Dead Sea basin (Torfstein et al., 2009a; Fig. 2a). However, as for our $\delta^{18}O$ record, no pollen data is available from ~12.5 to 11.9 ka and the question of climate conditions at Yammoûneh during the entire YD chronozone remains open.

5.4.3. The LGM period

During the cold period from 19 to 21 ka, when the EM water was ^{18}O-enriched by the glacial ice volume effect, inferred δ_L values at Yammoûneh were around −11‰ (about 2‰ lower than the modern water inflow, δ_I). In contrast, inferred $\delta_{cave\ water}$ values from Soreq suggests LGM values around −5‰, close to, or slightly higher than modern cave water values at this site (Fig. 13c,d). The different behavior of these two inland sites appears even more clearly when the two records are corrected for the "source effect" (Fig. 13e).

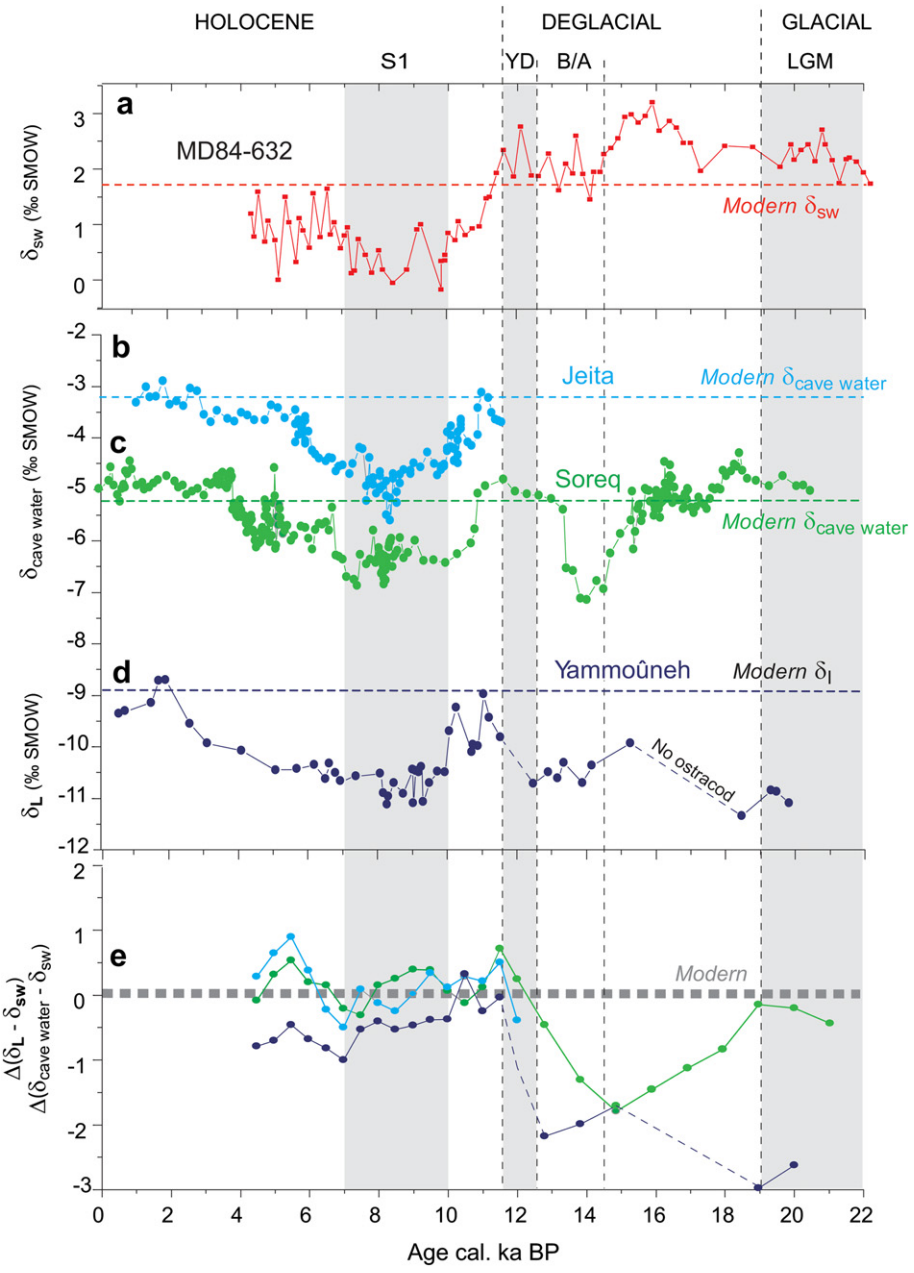

Fig. 13. Relationships between changes in the isotopic composition of sea surface water (δ_{sw}), lake and cave water. (a) δ_{sw} derived from SST_{alk} and $\delta^{18}O$ values of the foraminifera *G. ruber* in core MD84-632 (Essallami et al., 2007). (b–d) Reconstructed isotopic composition of Yammoûneh lake water (δ_L), as in Fig. 12b, Jeita Cave water (using data from Verheyden et al., 2008), and Soreq Cave water (using data from Bar-Matthews et al., 2003). (e) Difference between reconstructed lake or cave water and sea surface water isotopic composition [$\Delta(\delta_L - \delta_{sw})$, or $\Delta(\delta_{cave\ water} - \delta_{sw})$] normalized to modern.

Several factors may be invoked to explain low δ_L values at Yammoûneh at the LGM.

First, increased "continentality effect" on rainfall isotopic composition is unlikely because of the very steep bathymetric gradient off Lebanon at the latitude of Yammoûneh.

Second, our estimate of air temperature departure at the LGM may be wrong. Atmospheric temperature affected both the lake water temperature and rainfall isotopic composition, and thus δ_L. The effect of air temperature on δ_L can be easily tested: at Yammoûneh, an LGM δ_L close to the modern water inflow composition (as at Soreq) would imply temperature close to or higher than modern, which is not realistic. Furthermore, a regional synthesis of paleo-proxies has shown that during the LGM, the thermal atmospheric lapse rate was steeper than today over the circum-Mediterranean region (Kuhlemann et al., 2008). Terrestrial paleotemperature data used here (Fig. 12) come from low altitude sites (≤600 m a.s.l.) while Yammoûneh lies at 1360 m a.s.l., suggesting that the LGM ΔT value used here is underestimated. However, colder LGM lake water temperature at Yammoûneh would have increased the negative shift from the modern values even more. Conversely, low LGM δ_L values would be account for by the "ground-temperature effect" on rainfall isotopic composition (~0.58‰/°C at northern mid-latitudes; Rozanski et al., 1993). Colder atmospheric temperature combined with ^{18}O-enriched seawater can easily explain a δ_L depletion of 2‰ at Yammoûneh. Local thermal factors may have also partly contributed to the lake water depletion, but with little impact. Freezing of the Yammoûneh waterbody and surrounding soils over a long period of the year has inhibited evaporation, but evaporative enrichment

always remains low in this open lake basin. Most of the local precipitation was likely niveous, and thus more depleted than rain (Gat, 2000; Rozanski, 2005), including the small rains of the beginning and end of the wet season that are today enriched, but the basin is mainly supplied by snow melt-water even today.

Thirdly, enhanced moisture availability or "amount effect" might be invoked. According to Affek et al. (2008), LGM relative humidity was higher than today (60%) at the Soreq Cave site. Lisker et al. (2009) suggest that intervals with high P-E have occurred until ~17 ka in the Lisan–Dead Sea basin before the major Lateglacial aridification (Fig. 2a). However, the hypothesis of increased P-E balance at Yammoûneh at the LGM can be ruled out. Indeed, from ~16 to 21 ka, the sedimentary features suggest frequent periods of desiccation, and pollen data clearly indicate an open vegetation cover dominated by plants from steppe and desert reflecting very dry conditions (E. Van Campo, personal communication, 2009).

Lastly, changes in atmospheric circulation could also be considered. Data and simulations by general circulation models (e.g., Kageyama et al., 1999; Laîné et al., 2009) show that the northern mid-latitude westerly belt was pushed southward during the LGM in response to ice sheet and sea ice extent at northern high latitudes Although observations reveal that a straightforward zonal circulation may be too simplified and that meridional circulation systems should be considered during cold seasons (Kuhlemann et al., 2008), a southward displacement of low pressure cells lying today south of Italy and Turkey (Fig. 5) and low SSTs have likely affected the rainfall pattern and rainfall isotope composition in the Levant. Enzel et al. (2008) have suggested that, under glacial conditions, the Mediterranean cyclones coming from the northwest were forced to be funneled along the Mediterranean directly east into the Levant, explaining the high Late Pleistocene lake levels in the Lisan-Dead Sea basin (Fig. 2a). Today, at the event scale, the strongest rainfall depletion over Lebanon has been associated with air masses from the Atlantic entering the Mediterranean by the west (Aouad et al., 2005, Fig. 5). The dominance of storm tracks from the west might have contributed to the ^{18}O-depletion of water vapor reaching Lebanon.

To summarize, the ^{18}O-depletion of the Yammoûneh lake water at the LGM likely reflects the effect of a strong ground temperature decrease partly offset by the ^{18}O-enrichment of sea waters, and possibly associated with changes in air mass trajectories over the Mediterranean Sea imposed by glacial boundary conditions.

6. Conclusion

This paper provides the first paleo-environmental oxygen isotope record in the northern Levant, based on the isotopic composition of ostracod valves, for the last 21 ka. At Yammoûneh, the δ_c profile shows changes within a 2.5‰ range, with maximum and minimum values during the LGM and the early Holocene, respectively, and a slight late Holocene increase. This general trend is in agreement with other carbonate $\delta^{18}O$ records from the Mediterranean region. The Yammoûneh lake is in line with the conceptual model of an open lake system with fast discharge and low evaporative enrichment. Moreover, our data indicate that the isotopic composition of inflowing water to the lake basin is representative of the winter rainfall in the whole watershed. These hydrological specificities make the Yammoûneh lake suitable for exploring the effects of changes in temperature and in rainfall isotopic composition on the isotopic balance of an open lake in the eastern Mediterranean region.

In order to gain new insights about the factors controlling the terrestrial carbonate isotopic records, we have tentatively reconstructed a lake water isotopic (δ_L) record by correcting the δ_c values for: (1) the lake water temperature (using regional paleo-temperature estimates), and (2) the moisture "source effect". These corrections allow us to discuss the δ_L changes in term of several processes (amount effect, ground-temperature effect and other atmospheric features) that, in turn, imprint the carbonate isotopic composition. For comparison, we similarly reconstruct inland water composition from the δ_c records of speleothems from the northern and central Levant. During the Holocene period, the EM water isotope composition appears to have been the prime factor controlling the fluctuations of regional inland water composition. Nevertheless, during the period of the EM sapropel formation (~10–7.5 ka), the effect of low seawater isotope composition has probably been reinforced by enhanced inland rainfall (amount effect) leading to the most depleted $\delta^{18}O$ values of the whole record. During the LGM, the δ_L depletion at Yammoûneh does not fingerprint the seawater isotopic enrichment, in contrast with Soreq Cave water, and cannot be attributed to increased rainfall. This depletion is likely due to the negative ground-temperature effect enhanced by a steeper thermal altitudinal gradient, possibly associated with changes in air mass trajectories over the Mediterranean Sea. This suggests that, at least in open lake systems, the source area effects during the Holocene and glacial–interglacial temperature changes have been important drivers on inland ^{18}O isotope signals in the EM Mediterranean region.

Our data suggest some differences in the climate evolution of the northern and southern Levant (e.g., during the B/A period or around 8 ka). They may reflect changes in atmospheric circulation similar to those explaining modern changes in N–S precipitation gradients. However, a detailed comparison with other records from eastern Mediterranean sites would needs further work in order to obtain higher resolution and reliable data from the source area (e.g. δ_{sw}) as well as multiproxy paleoclimate time series from the northern Levant (including reliable continental temperature reconstructions).

Our approach includes many assumptions and should only be regarded as a tentative and qualitative approach for testing the potential effects of temperature and moisture source composition on the terrestrial carbonate $\delta^{18}O$ record. The presented results suffer large uncertainties due to, among other factors, uncertainties on our late Pleistocene chronology, the lack of accurate paleotemperature estimates from both terrestrial and marine sites from the eastern Mediterranean region, and to our poor understanding of seasonal changes in the Yammoûneh paleo-lake. Results presented here do not presume to represent absolute values, but major trends and differences from modern for the relatively well-constrained early Holocene and LGM periods can be regarded as significant. We have shown that comparing δ_L records rather than δ_c records helps to disentangle the factors controlling the terrestrial isotopic records.

Acknowledgements

We are grateful to P. Tapponnier, IPG-P, who has initiated the investigation of the Yammoûneh basin for both tectonic and paleo-environmental purposes. We thank our colleagues from the IPG-P and from the Centre National de Recherches Géophysiques from Lebanon for their help during fieldwork and for fruitful discussions. In particular, we thank M. Daëron who has sampled charcoals in the trenches and provided us with a set of unpublished ^{14}C dates. Thanks are due to M. Massault, CEN Saclay, Gif-sur-Yvette, who has performed ^{14}C measurements from our water samples, to several colleagues from the CEREGE: C. Vallet-Coulomb for ^{18}O and D analyses on modern waters, C. Sonzogni for her help in oxygen analysis on carbonate, D. Williamson for magnetic susceptibility analyses, and C. Paillès for her help in the field and description of the sedimentary profiles. We are also grateful to the SETEL company to have conducted the coring mission. We thank F.H. Nader, K.-C. Emeis, N. Kallel and M.-A. Sicre, EPSL, for kindly providing data files on Jeita Cave and marine cores. Support from

this study came from the CNRS-France, the CNRS-Lebanon, the French Embassy in Lebanon, and the CEDRE French-Lebanese program (convention no. 03 En F34/L42). We are grateful to two anonymous reviewers who spent time to provide constructive comments and suggestions which helped us to deeply improve the manuscript.

Appendix. Supplementary data

Supplementary data associated with this article can be found in the online version, at doi:10.1016/j.quascirev.2009.12.005

References

Abd-el-Ab, I., 1967. Statique et dynamiques des eaux dans les masifs calcaires libano-syriens. Chronique d'Hydrogéologie 10, 75–94.
Abi-Saleh, B., Safi, S., 1988. Carte de la végétation du Liban. Ecologia Mediterranea 14, 123–141.
Affek, H.P., Bar-Matthews, M., Ayalon, A., Matthews, A., Eiler, J.M., 2008. Glacial/interglacial temperature variations in Soreq cave speleothems as recorded by "clumped isotope" thermometry. Geochimica et Cosmochimica Acta 72 (22), 5351–5360.
Almogi-Labin, A., Bar-Matthews, M., Shriki, D., Kolosovsky, E., Paterne, M., Schilman, B., Ayalon, A., Aiznshtat, Z., Matthews, A., in press. Climatic variability during the last ~90 ka on the southern and northern Levantibe basin as evident from marine records and speleothems. Quaternary Science Reviews, in press.
Aouad, A., Travi, Y., Blavoux, B., Job, J.O., Najem, W., 2004. Etude isotopique de la pluie et de la neige sur le Mont Liban: premiers résultats. Hydrological Sciences 49, 429–441.
Aouad, A., Job, J.O., Khalil, S., Touma, T., Bitar, C., Bocquillon, C., Najem, W., 2005. Snow in Lebanon: a preliminary study of snow cover over Mount Lebanon and a simple snowmelt model. Hydrological Sciences 50 (3), 555–569.
Bar-Matthews, M., Ayalon, A., Kaufman, A., 1997. Late quaternary paleoclimate in the Eastern Mediterranean region from stable isotope analysis of speleothems at Soreq cave. Israel. Quaternary Research 47, 155–168.
Bar-Matthews, M., Ayalon, A., Kaufman, A., Wasserburg, G.J., 1999. The Eastern Mediterranean paleoclimate as a reflection of regional events: Soreq cave, Israel. Earth and Planetary Science Letters 166 (1–2), 85–95.
Bar-Matthews, M., Ayalon, A., Gilmour, M., Matthews, A., Hawkesworth, C.J., 2003. Sea-land oxygen isotopic relationship from planktonic foraminifera and speleothems in the Eastern Mediterranean region and their implication for paleorainfall during interglacial intervals. Geochimica et Cosmochimica Acta 67 (17), 3181–3199.
Bartov, Y., Stein, M., Enzel, Y., Agnon, A., Reches, Z., 2002. Lake levels and Sequence stratigraphy of lake Lisan, the late Pleistocene precursor of the Dead Sea. Quaternary Research 57 (1), 9–21.
Bartov, Y., Goldstein, S.L., Mordechai, S., Enzel, Y., 2003. Catastrophic arid episodes in the Eastern Mediterranean linked with the North Atlantic Heinrich events. Geology 31 (5), 439–442.
Bar-Yosef, O., 1998. The Natufian Culture in the Levant. Threshold to the origins of agriculture. Evolutionary Anthropology 6, 169–177.
Belis, C.A., Ariztegui, D., 2004. The influence of biological and environmental factors on the stable isotopic composition of ostracods – the late Pleistocene record from Lake Albano, Central Italy. Journal of Limnology 63 (2), 219–232.
Besançon, J., 1968. Le poljé de Yammoûné. Revue Libanaise de Géographie 3, 3–62.
Blunier, T., Brook, K., 2001. Synchronization of the Byrd and Greenland (GISP2/GRIP) Records. IGBP PAGES/World Data Center-A for Palaeoclimatology, Data Contribution Series #2001-003, NOAA/NGDC Palaeoclimatology Program, Boulder, CO.
Bookman, R., Bartov, Y., Enzel, Y., Stein, M., 2006. The levels of the late Quaternary lakes in the Dead Sea basin: two centuries of research. In: Enzel, Y., Agnon, A., Stein, M. (Eds.), New Frontiers in Dead Sea Paleoenvironmental Research. Geological Society of America Special Paper 401, pp. 155–170.
Bowen, G.J., Revenaugh, J., 2003. Interpolating the isotopic composition of modern meteoric precipitation. Water Resources Research 39 (10), 1299–1312.
Bowen, G.J., Wilkinson, B., 2002. Spatial distribution of $\delta^{18}O$ in meteoric precipitation. Geology 30 (4), 315–318.
Bowen, G.J., Wassenaar, L.I., Hobson, K., 2005. Global application of stable hydrogen and oxygen isotopes to wildlife forensics. Oecologia 143, 337–348.
Bronshtein, Z.S., 1947. Fresh-water Ostracoda. Fauna of the USSR. Crustaceans, vol. 2. Academy of Sciences of the USSR, Moscow, 470 pp.
Cappers, R.T.J., Bottema, S., Woldring, H., van der Plicht, H., Streurman, H.J., 2002. Modelling the emergence of farming: implications of the vegetation development in the Near East during the Pleistocene/Holocene transition. In: Cappers, R.T.J., Bottema, S. (Eds.), The Dawn of Farming in the Near East. Oxbow Books, Oxford, UK.
Craig, H., 1961. Isotopic variations in meteoric waters. Science 133, 1702–1703.
Craig, H., Gordon, L.I., 1965. Deuterium and oxygen-18 variations in the ocean and the marine atmosphere, in: Tongiorgi, E. (Ed.), Stable Isotopes in Oceanographic Studies and Paleotemperatures. Consigilio Nazionale delle Ricerche, Laboratorio di Geologia Nucleare, Pisa, pp. 9–130.
Daëron, M., 2005. Rôle, cinématique et comportement sismique à long terme de la faille de Yammoûneh, principale branchedécrochante du coude transpressif libanais (faille du Levant). Thesis, Paris 6 University.
Daëron, M., Benedetti, L., Tapponnier, P., Sursock, A., Finkel, R.C., 2004. Constraints on the post-25-ka slip rate of the Yammoûneh fault (Lebanon) using in situ cosmogenic ^{36}Cl dating of offset limestone-clast fans. Earth and Planetary Science Letters 227 (1–2), 105–119.
Daëron, M., Klinger, Y., Tapponnier, P., Elias, A., Jacques, E., Sursock, A., 2007. 12,000-year-long record of 10 to 13 paleoearthquakes on the Yammoûneh fault, Levant fault system. Lebanon. Bulletin of the Seismological Society of America 97 (3), 749–771.
Dansgaard, W., 1964. Stable isotopes in precipitation. Tellus 16, 438–468.
Davis, B.A.S., Brewer, S., Stevenson, A.C., Guiot, J., Contributors, Data, 2003. The temperature of Europe during the Holocene reconstructed from pollen data. Quaternary Science Reviews 22, 1701–1716.
Develle, A.-L., Williamson, D., Gasse, F., Walter-Simonnet, A.-V., 2009. Early Holocene volcanic ash fallout in the Yammoûneh lacustrine basin (Lebanon). Tephrochronological implications for the Near-East. Journal of Volcanology and Geothermal Research 186, 416–425.
Dubertret, L., 1975. Introduction à la carte géologique au 1/50 000 du Liban. Notes et Mémoires du Moyen-Orient 13, 345–403.
Dubowski, Y., Erez, J., Stiller, M., 2003. Isotopic paleolimnology of Lake Kinneret. Limnology and Oceanography 48, 68–78.
Dügel, M., Külköylüolu, O., Kýlýç, M., 2008. Species assemblages and habitat preferences of Ostracoda (Crustacea) in Lake Abant (Bolu, Turkey). Belgian Journal of Zoology 138 (1), 50–59.
el Hakim, M., 2005. Les aquifères karstiques de l'Anti-Liban et du nord de la plaine de la Beqaa: caractéristiques, fonctionnement, évolution et modélisation, d'après l'exemple du système karstique Anjar-Chamsine (Liban). Thesis, Université Montpellier II, Montpellier, Université Saint Joseph, Beyrouth, 215 pp.
Emeis, K.C., Struck, U., Schulz, H.M., Rosenberg, R., Bernasconi, S., Erlenkeuser, H., Sakamoto, T., Martinez-Ruiz, F., 2000. Temperature and salinity variations of Mediterranean Sea surface waters over the last 16,000 years from records of planktonic stable oxygen isotopes and alkenone unsaturation ratios. Palaeogeography, Palaeoclimatology, Palaeoecology 158 (3-4), 259–280.
Emeis, K.C., Schulz, H., Struck, U., Rossignol-Strick, M., Erlenkeuser, H., Howell, M.W., Kroon, D., Mackensen, A., Ishizuka, S., Oba, T., Sakamoto, T., Koizumi, I., 2003. Eastern Mediterranean surface water temperatures and $\delta^{18}O$ during deposition of sapropels in the late Quaternary. Paleoceanography 18 (1), 1005. doi:10.1029/2000PA000617.
Enzel, Y., Bookman, R., Sharon, D., Gvirtzman, H., Dayan, U., Baruch, Z., Stein, M., 2003. Late Holocene climates of the Near East deduced from Dead Sea level variations and modern regional winter rainfall. Quaternary Research 60 (3), 263–373.
Enzel, Y., Amit, R., Dayan, U., Crouvi, O., Kahana, R., Baruch, Z., Sharon, D., 2008. The climatic and physiographic controls of the eastern Mediterranean over the late Pleistocene climates in the southern Levant and its neighboring deserts. Global and Planetary Change 60, 165–192.
Essallami, L., Sicre, M.A., Kallel, N., Labeyrie, L., Siani, G., 2007. Hydrological changes in the Mediterranean Sea over the last 30,000 years. Geochemistry Geophysics Geosystems 8 (7). doi:10.1029/2007GC001587.
Farrera, I., Harrison, S.P., Prentice, I.C., Ramstein, G., Guiot, J., Bartlein, P.J., Bonnefille, R., Bush, M., Cramer, W., von Grafenstein, U., Holmgren, K., Hooghiemstra, H., Hope, G., Jolly, D., Lauritzen, S.E., Ono, Y., Pinot, S., Stute, M., Yu, G., 1999. Tropical climates at the Last Glacial Maximum: a new synthesis of terrestrial palaeoclimate data. I. Vegetation, lake-levels and geochemistry. Climate Dynamics 15, 823–856.
Filippi, M.L., Lambert, P., Hunziker, J., Kübler, B., Bernasconi, S., 1999. Climatic and anthropogenic influence on the stable isotope record from bulk carbonates and ostracodes in Lake Neuchâtel, Switzerland, during the last two millennia. Journal of Paleolimnology 21 (1), 19–34.
Fontugne, M.R., Calvert, S.E., 1992. Late Pleistocene variability of the carbon isotopic composition of organic matter in the eastern Mediterranean: monitor of changes in carbon sources and atmospheric CO_2 concentrations. Paleoceanography 7 (1), 1–20.
Fontugne, M., Arnold, M., Labeyrie, L., Paterne, M., Calvert, S.E., Duplessy, J.C., 1994. Palaeoenvironment Sapropel chronology and Nile river discharge during the last 20 000 years as indicated by deep sea sediment records in the Eastern Mediterranean, in: Bar-Yosef, O., Kra, R.S. (Eds.), Late Quaternary Chronology and Paleoclimates of the Eastern Mediterranean. Radiocarbon, Tucson, AZ, pp. 75–88.
Frumkin, A., Ford, D.C., Schwarcz, H.P., 1999. Continental oxygen isotopic record of the last 170,000 years in Jerusalem. Quaternary Research 51 (3), 317–327.
Frumkin, A., Ford, D.C., Schwarcz, H.P., 2000. Paleoclimate and vegetation of the last glacial cycles in Jerusalem from a speleothem record. Global Biochemical Cycles 14 (3), 863–870.
Gat, J.R., 1995. Stable isotopes of fresh and saline lakes. In: Lerman, A., Imboden, D., Gat, J.R. (Eds.), Physics and Chemistry of Lakes. Springer, Berlin, pp. 139–166.
Gat, J.R., 1996. Oxygen and hydrogen isotopes in the hydrologic cycle. Annual Review of Earth and Planetary Sciences 24, 225–262.
Gat, J.R., 2000. Atmospheric water balance – the isotopic perspective. Hydrological Processes 14 (8), 1357–1369.
Gat, J.R., Carmi, I., 1970. Evolution of the isotopic composition of atmospheric waters in Mediterranean Sea area. Journal of Geophysical Research 75, 3039–3078.
Gat, J.R., Carmi, I., 1987. Effect of climate changes on the precipitation patterns and isotopic composition of water in a climate transition zone: case of the Eastern

Mediterranean Sea area. International Association of Hydrological Sciences Publication 168, 513–523.
Gat, J.R., Klein, B., Kushnir, Y., Roether, W., Wernli, H., Yam, R., Shemesh, A., 2003. Isotope composition of air moisture over the Mediterranean Sea: an index of the air–sea interaction pattern. Tellus Series B-Chemical and Physical Meteorology 55 (5), 953–965.
Gonfiantini, R., 1986. Environmental isotopes in lake studies. In: Fritz, P., Fontes, J.C. (Eds.), Handbook of Environmental Isotope Geochemistry. The Terrestrial Environment, vol. 2. B. Elsevier, Amsterdam, pp. 113–168.
Haase-Schramm, A., Goldstein, S.L., Stein, M., 2004. U-Th dating of Lake Lisan (late Pleistocene Dead Sea) aragonite and implications for glacial East Mediterranean climate change. Geochimica et Cosmochimica Acta 68 (5), 985–1005.
Hajar, L., Khater, C., Cheddadi, R., 2008. Vegetation changes during the late Pleistocene and Holocene in Lebanon: a pollen record from the Beqaa Valley. The Holocene 18 (7), 1089–1099.
Hakim, B., 1985. Recherches hydrologiques et hydrochimiques sur quelques karsts méditerranéens. Liban, Syrie et Maroc. Université Libanaise, Section des Etudes Géographiques II, Beyrouth.
Haslett, J., Parnell, A., 2008. A simple monotone process with application to radiocarbon-dated depth chronologies. Journal of the Royal Statistical Society Series C-Applied Statistics 57, 399–418.
Hayes, A., Kucera, M., Kallel, N., Sbaffi, L., Rohling, E.J., 2005. Glacial Mediterranean sea surface temperatures based on planktonic foraminiferal assemblages. Multiproxy Approach for the Reconstruction of the Glacial Ocean surface. Quaternary Science Reviews 24 (7–9), 999–1016.
Hazan, N., Stein, M., Agnon, A., Marco, S., Nadel, D., Negendank, J.F.W., Schwab, M.J., Neev, D., 2005. The late Quaternary limnological history of Lake Kinneret (Sea of Galilee), Israel. Quaternary Research 63 (1), 60–77.
Hiller, D., 1972. Untersuchugen zur Biologie un zur Ökologie limnischer Ostracoden aus der umgeung von Hamburg. Archives of Hydrobiology Supplement 40, 400–497.
Horowitz, A., 1979. The Quaternary of Israel. Academic Press, New York, 394 pp.
Issar, A.S., Zohar, M., 2004. Climate Change. Environment and Civilization in the Middle East. Springer-Verlag, Berlin.
Kageyama, M., Valdes, P.J., Ramstein, G., Hewitt, C., Wyputta, U., 1999. Northern hemisphere storm tracks in present day and Last Glacial Maximum climate simulations: A comparison of the European PMIP models. Journal of Climate 12, 742–760.
Kallel, N., Paterne, M., Duplessy, J.-C., Vergnaud-Grazzini, C., Pujol, C., Labeyrie, L., Arnold, M., Fontugne, M., Pierre, C., 1997. Enhanced rainfall in the Mediterranean region during the last sapropel event. Oceanologica Acta 20, 697–712.
Karam, F., 2002. Climate change and variability in Lebanon: impact on land use and sustainable agriculture development, in: Proceedings of the First Technical Workshop of the "Mediterranean" Component of CLIMAGRI Project on Climate Change and Agriculture, 25-27 September. FAO, Rome.
Kolodny, Y., Stein, M., Machlus, M., 2005. Sea-rain-lake relation in the Last Glacial East Mediterranean revealed by $\delta^{18}O \sim {}^{13}C$ in Lake Lisan aragonites. Geochimica et Cosmochimica Acta 69, 4045–4060.
Kuhlemann, J., Rohling, E.J., Krumrei, I., Kubik, P., Ivy-Ochs, S., Kucera, M., 2008. Regional synthesis of Mediterranean atmospheric circulation during the Last Glacial Maximum. Science 231, 1338–1340.
Külköylüolu, O., Yilmaz, F., 2006. Ecological requirements of Ostracoda (Crustacea) in three types of springs in Turkey. Limnologica 36 (3), 172–180.
Lachniet, M.S., 2009. Climatic and environmental controls on speleothem oxygen-isotope values. Quaternary Science Reviews 28, 412–432.
Laîné, A., Kageyama, M., Salas-Mélia, D., Voldoire, A., Rivière, G., Ramstein, G., Planton, S., Tyteca, S., Peterschmitt, J.Y., 2009. Northern hemisphere storm tracks during the last glacial maximum in the PMIP2 ocean-atmosphere coupled models: energetic study, seasonal cycle, precipitation. Climate Dynamics 32, 593–614. doi:10.1007/s00382-008-0391-9.
Leng, M.J., Marshall, J.D., 2004. Palaeoclimate interpretation of stable isotope data from lake sediment archives. Quaternary Science Reviews 23 (7–8), 811–831.
Levitus, S., Boyer, T.P., 1994. World Ocean Atlas 1994. National Oceanographic Data Center, Silver Spring, MD.
Lisker, S., Vaks, A., Bar-Matthews, M., Porat, R., Frumkin, A., 2009. Stromatolites in caves of the Dead Sea Fault Escarpment: implications to latest Pleistocene lake levels and tectonic subsidence. Quaternary Science Reviews 28 (1–2), 80–92.
McGarry, S., Bar-Matthews, M., Matthews, A., Vaks, A., Schilman, B., Ayalon, A., 2004. Constraints on hydrological and paleotemperature variations in the Eastern Mediterranean region in the last 140 ka given by the δ *D* values of speleothems fluid inclusions. Quaternary Science Reviews 23, 919–934.
Meisch, C., 2000. Freshwater Ostracoda of Western and Central Europe. Spektrum Akademischer Verlag, Heidelberg, Berlin.
Mezquita, F., Tapia, G., Roca, J.R., 1999. Ostracoda from springs on the eastern Iberian Peninsula: ecology, biogeography and paleolimnological implications. Palaeogeography, Palaeoclimatology, Palaeoecology 148, 65–85.
Migowski, C., Stein, M., Prasad, S., Negendank, J.F.W., Agnon, A., 2006. Holocene climate variability and cultural evolution in the Near East from the Dead Sea sedimentary record. Quaternary Research 66 (3), 421–431.
Mix, A.C., Bard, E., Schneider, R., 2001. Environmental processes of the ice age: land, oceans, glaciers (EPILOG). Quaternary Science Reviews 20 (4), 627–657.
Nader, F.H., Verheyden, S., Cheng, H., Swennen, R., 2007. Etude pétrographique et géochimique d'une stalagmite de la grotte de Jeita (Liban). Lebanese Science Journal 8 (2), 45–58.
Park, L.E., Cohen, A.S., Martens, K., Bralek, R., 2003. The impact of taphonomic processes on interpreting paleoecologic changes in large lake ecosystems: ostracodes in Lakes Tanganyika and Malawi. Journal of Paleolimnology 30 (2), 127–138.
Reimer, P.J., Baillie, M.G., Bard, E., Bayliss, A., Beck, W.W., Bertrand, C.J., Blackwell, P.G., Buck, C.E., Burr, G.S., Cutler, K.B., Damon, P.E., Edwards, L.L., Fairbanks, R.G., Friedrich, M., Guilderson, T.P., Hogg, A.G., Hughen, K.A., Kromer, B., Mccormac, G., Manning, S., Ramsey, C.B., Reimer, R.W., Remmele, S., Southon, J.R., Stuiver, M., Talamo, S., Taylor, F., van der Plicht, J., Weyhenmeyer, C.E., 2005. IntCal04 terrestrial radiocarbon age calibration, 0–26 cal kyr BP. Radiocarbon 46 (3), 1029–1058.
Ricketts, R.D., Johnson, T.C., Brown, E.T., Rasmussen, K.A., Romanovsky, V.V., 2001. The Holocene paleolimnology of Lake Issy-Kul, Kyrgyzstan: trace elements and stable isotope composition of ostracodes. Palaeogeography, Palaeoclimatology, Palaeoecology 176, 207–227.
Rindsberger, M., Magaritz, M., Carmi, I., Gilad, D., 1983. The Relation between air-mass trajectories and the water isotope composition of rain in the Mediterranean Sea Area. Geophysical Research Letters 10 (1), 43–46.
Rindsberger, M., Jaffe, Sh., Rahamim, Sh., Gat, J.R., 1990. Patterns of the isotopic composition of precipitation in time and space: data from the Israeli storm water collection program. Tellus 42B, 263–271.
Röhling, E.J., 1994. Review and new aspects concerning the formation of eastern Mediterranean sapropels. Marine Geology 122, 1–28.
Roberts, N., Jones, M.D., Benkaddour, A., Eastwood, W.J., Filippi, M.L., Frogley, M.R., Lamb, H.F., Leng, M.J., Reed, J.M., Stein, M., Stevens, L., Valero-Garcés, B., Zanchetta, G., 2008. Stable isotope records of Late Quaternary climate and hydrology from Mediterranean lakes: the ISOMED synthesis. Quaternary Science Reviews 27 (25–26), 2426–2441.
Robinson, A.S., Black, S., Sellwood, B.W., Valdes, P.J., 2006. A review of palaeoclimates and palaeoenvironments in the Levant and Eastern Mediterranean from 25,000 to 5,000 years BP: setting the environmental background for the evolution of human civilisation. Quaternary Science Reviews 25, 1617–1641.
Roca, J.R., Baltanàs, A., 1993. Ecology and distribution of Ostracoda in Pyrenean springs. Journal of Crustacean Biology 13 (1), 165–174.
Rozanski, K., 2005. Isotopes in atmospheric moisture. In: Aggarwal, P.K., Gat, J.R., Froehlich, K.F. (Eds.), Isotopes in the Water Cycle: Past, Present and Future of a Developing Science. Springer, Dordrecht, pp. 291–302.
Rozanski, K., Araguás-Araguás, L., Gonfiantini, R., 1992. Relation between long-term trends of oxygen-18 isotope composition of precipitation and climate. Science 258 (5084), 981–985.
Rozanski, K., Araguas-Araguas, L., Gonfiantini, R., 1993. Isotopic patterns in modern global precipitation, in: Climate Change in Continental Isotopic Records, Geophysical Monograph 78. American Geophysical Union, Washington, DC. pp. 1–36.
Safi, S., Abi-Saleh, B., 1999. Assessment of Lebanon's vulnerability to climate change: Technical annex B4: terrestrial ecosystems and natural habitats. In: Lebanon's First National Communication under the United Nations Framework Convention on Climate Change. Ministry of Environment, Lebanon.
Schwalb, A., 2003. Lacustrine ostracodes as stable isotope recorders of late-glacial and Holocene environmental dynamics and climate. Journal of Paleolimnology 29, 267–351.
Service Météorologique du Liban, 1977. Atlas Climatique du Liban. Service Météorologique du Liban, Beirut, Lebanon.
Sharon, D., Kutiel, H., 1986. The distribution of rainfall intensity in Israel, its regional and seasonal variations and its climatological evaluation. Journal of Climatology 6, 277–291.
Siegenthaler, U., Eicher, U., 1986. Stable oxygen and carbon isotope analyses. In: Berglund, B.E. (Ed.), Handbook of Holocene Palaeoecology and Palaeohydrology. Wiley, Chichester, pp. 407–422.
Stiller, M., Hutchinson, G.E., 1980. The Waters of Merom: a study of Lake Huleh VI. Stable isotope composition of carbonates of a 54 m core: paleoclimatic and paleotrophic implications. Archives of Hydrobiology 89, 275–302.
Stiller, M., Kaufman, A., 1985. Paleoclimatic trends revealed by the isotopic composition of carbonates in Lake Kinneret. Zeitschrift für Gletscherkunde 21, 79–87.
Talbot, M.R., 1990. A review of paleohydrological interpretation of carbon and oxygen isotopic ratios in primary lacustrine carbonates. Chemical Geology (Isotopes Geoscience Section) 80, 261–279.
Torfstein, A., Stein, M., Yechieli, J., 2009a. Dry-spells in the Levant During the Last Deglaciation Identified by Dead Sea LakeLevels. AGU Chapman Conference on Abrupt Climate Change, 15–19 June 2009, Abstract. Columbus, OH.
Torfstein, A., Haase-Schramm, A., Waldmann, N., Kolodny, Y., Stein, M., 2009b. U-series and oxygen isotope chronology of the mid-Pleistocene Lake Amora (Dead Sea basin). Geochimica et Cosmochimica Acta 73, 2603–2630.
Verheyden, S., Nader, F.H., Cheng, H.J., Edwards, L.R., Swennen, R., 2008. Paleoclimate reconstruction in the Levant region from the geochemistry of a Holocene stalagmite from the Jeita cave. Lebanon. Quaternary Research 70 (3), 368–381.
Von Grafenstein, U., Erlenkeuser, H., Müller, J., Kleinmann-Eisenmann, A., 1992. Oxygen isotope records of benthic ostracods in Bavarian lake sediments (reconstruction of late and post Glacial air temperatures). Naturwissenschaften 79, 145–152.
Von Grafenstein, U., Erlenkeuser, H., Trimborn, P., 1999. Oxygen and carbon isotopes in modern fresh-water ostracod valves: assessing vital offsets and autecological effects of interest for palaeoclimate studies. Palaeogeography, Palaeoclimatology, Palaeoecology 148, 133–152.

Wilkinson, I.P., Bubikyan, S.A., Gulakyan, S.Z., 2005. The impact of late Holocene environmental change on lacustrine Ostracoda in Armenia. Earth Environments and Dynamics of Ostracoda – Earth Environments and Dynamics of Ostracoda. Palaeogeography, Palaeoclimatology, Palaeoecology 225 (1–4), 187–202.

Wolf, J.P., 1920. Die Ostrakoden aus der Umgebung von Basel. Archiv für Naturgeschichte 85 (3), 1–100.

Wu, H.B., Guiot, J.L., Brewer, S., Guo, Z.T., 2007. Climatic changes in Eurasia and Africa at the last glacial maximum and mid-Holocene: reconstruction from pollen data using inverse vegetation modelling. Climate Dynamics 29 (2–3), 211–229.

Xia, J., Ito, E., Engstrom, D.R., 1997a. Geochemistry of ostracode calcite: Part 1. An experimental determination of oxygen isotope fractionation. Geochimica et Cosmochimica Acta 61, 377–382.

Xia, J., Engstrom, D.R., Ito, E., 1997b. Geochemistry of ostracode calcite: Part 2. The effects of water chemistry and seasonal temperature variation on *Candona rawsoni*. Geochimica et Cosmochimica Acta 61, 383–391.

Yasuda, Y., Kitagawa, H., Nakagawa, T., 2000. The earliest record of major anthropogenic deforestation in the Ghab Valley, northwest Syria: a palynological study. Quaternary International 73/74, 127–136.

Zangvil, A., Karas, S., Sasson, A., 2003. Connection between eastern Mediterranean seasonal mean 500 HPA height and sea level pressure patterns and the spatial rainfall distribution over Israel. International Journal of Climatology 23, 1567–1576.

Ziv, B., Dayan, U., Kuschnir, Y., Roth, C., Enzel, Y., 2006. Regional and global atmospheric patterns governing rainfall in the southern Levant. International Journal of Climatology 26, 55–73.